



Metal source and fluid–rock interaction in the Archean BIF-hosted Lamego gold mineralization: Microthermometric and LA-ICP-MS analyses of fluid inclusions in quartz veins, Rio das Velhas greenstone belt, Brazil



Milton J. Morales^{a,*}, Rosaline C. Figueiredo e Silva^a, Lydia M. Lobato^a, Sylvio D. Gomes^a, Caio C.C.O. Gomes^b, David A. Banks^c

^a Universidade Federal de Minas Gerais, CPMTc-Instituto de Geociências, Av. Presidente Antônio Carlos, 6627, Pampulha, Belo Horizonte, MG, Brazil

^b AngloGold Ashanti Córrego do Sítio Mineração S/A, Lamego Mine, Rua Mestre Caetano, Sabará, MG, Brazil

^c School of Earth and Environment, University of Leeds, Woodhouse Lane, Leeds LS2 9JT, United Kingdom

ARTICLE INFO

Article history:

Received 7 May 2015

Received in revised form 7 August 2015

Accepted 15 August 2015

Available online 21 August 2015

Keywords:

Quadrilátero Ferrífero

Fluid inclusions

LA-ICP-MS

Hydrothermal alteration

Quartz veins

Metamorphic fluids

ABSTRACT

The Lamego orogenic gold deposit (440,742 oz gold measured reserves and 2.4 million t measured resources, with an average grade of 5.71 g/t Au and a cut-off grade of 2.15 g/t Au; AngloGold Ashanti Córrego do Sítio Mineração S/A (AGA) personal communication, 2014) is located in the 5 km-long trend that includes the world-class Cuibá deposit. It is hosted in the Neoproterozoic metavolcano–sedimentary rocks of the Rio das Velhas greenstone belt, Quadrilátero Ferrífero, Brazil. Mineralization is associated mainly with metachert–banded iron formation (BIF) and carbonaceous phyllites in the reclined Lamego fold, in which the Cabeça de Pedra orebody represents the hinge zone. Mineralization is concentrated in silicification zones and their quartz veins, as well as in sulfide minerals, product of BIF sulfidation. Hydrothermal alteration varies according to host rock, with abundant sulfide–carbonate in BIF, and sericite–chlorite in carbonaceous phyllite. Quartz vein classification according to structural relationships and host rocks identified three vein systems. The V1 system, mainly composed of smoky quartz (Qtz I) and pyrite, is extensional, crosscuts the bedding plane S_0 of BIF, and is parallel to the fold axis. The V2 system, of the same composition, is represented by veins that are parallel to the S_{1-2} foliation and S_0 . This system is also characterized by silicification zones in the BIF–carbonaceous phyllite contact that has its maximum expression in the hinge zone of folds. The V3 system has milky quartz (Qtz II) veins, which result from the recrystallization of smoky quartz, located mainly in shear zones and faults; these veins form structures en echelon and vein arrays. The most common ore minerals are pyrite, As-pyrite and arsenopyrite. Fluid inclusion-FI trapped in all quartz veins present composition in the $H_2O-CO_2 \pm CH_4-NaCl$ system. Fluid evolution can be interpreted in two stages: i) aqueous–carbonic fluid trapped in Qtz I, of low salinity (~2% equiv. wt.% NaCl), and ii) carbonic–aqueous fluid, of moderate salinity (average 9 eq. wt.% NaCl) hosted in Qtz II. Both stages are characterized by decrepitation temperatures in the range of 200 to >300 °C, and suggest a fluid of metamorphic origin. Applying an arsenopyrite geothermometer, the calculated formation temperature for the Cabeça de Pedra orebody is 300 to 375 °C. The vertical intersection of the isochors allows a minimum pressure calculation of 2.6 kbar. The composition of individual FIs of this orebody, obtained by LA-ICP-MS analyses, compared with results of FIs for the Carvoaria Velha deposit, Córrego do Sítio lineament, highlights a standard composition typical of metamorphic fluids with $Na > K > Ca > Mg$, which increase or decrease in concentration as a function of salinity in both deposits. Trace elements vary according to fluid–rock reactions, and are directly related to the host rock composition. The comparison of data sets of the two deposits shows that the Cabeça de Pedra FIs have a higher enrichment in Zn, while Cu, As and Sb are richer in Carvoaria Velha, suggesting influence of the host rock geochemistry. The suggested mechanisms for gold precipitation at the Cabeça de Pedra orebody, Lamego gold deposit are: i) hydrolysis of the carbonaceous matter of phyllite and BIF, affecting fO_2 , destabilizing sulfur complexes and enhancing gold precipitation; ii) replacement of BIF iron carbonates by sulfides; and iii) continuous pressure changes that lead to silica precipitation and free gold. Other than playing the long-recognized role of the carbonaceous phyllites as a fluid barrier, the data highlight their importance as a source of metals.

© 2015 Elsevier B.V. All rights reserved.

* Corresponding author.

E-mail address: mjulianmorales@gmail.com (M.J. Morales).

1. Introduction

The Neoproterozoic Rio das Velhas greenstone belt represents a supra-crustal sequence, which had its tectonomagmatic activity peak between 2780–2700 Ma (Noce et al., 2007). It hosts world-class orogenic (Groves et al., 1998) gold deposits, and has historically been studied with exploration purposes since the Portuguese colonization of Brazil in the seventeenth and eighteenth centuries, the so-called gold cycle (Russell-Wood, 1984).

Geographically located in the central-south part of the state of Minas Gerais, southeast of Brazil, the Quadrilátero Ferrífero (QF) mineral district is part of the extreme south of the Craton São Francisco (Almeida, 1967; Almeida and Hasui, 1984), comprising three main units: granite–gneiss terrains; the Rio das Velhas greenstone belt; and Proterozoic metasedimentary sequences (Dorr, 1969; Dorr et al., 1957). The Rio das Velhas Supergroup, host to the largest number of gold deposits in the QF (Lobato et al., 2001a, 2001b), is divided into the 1) Nova Lima Group, composed of a metavolcano–sedimentary sequence, and 2) Maquiné Group, composed of continental clastic sequences (Baltazar and Zucchetti, 2007).

The different gold deposits in the region were formed during the Archean deformation that affected the Rio das Velhas Supergroup, associated with large volumes of hydrothermal fluids (e.g., Ribeiro-Rodrigues et al., 2007; Vial et al., 2007a,b), which are correlated in age and background characteristics with other deposits present in different cratons of the world (Goldfarb et al., 2001, 2005). World-class deposits such as Morro Velho (>500 t) and Cuiabá (>100 t), and smaller ones such as Raposos, Juca Vieira, São Bento, Córrego do Sítio and Lamego are hosted in different rocks of the Nova Lima Group, and present varying mineralization styles (Lobato et al., 1998, 2001b).

The Lamego gold deposit is situated in the town of Sabará (Fig. 1), some 5 km from the world-class Cuiabá deposit. It is exploited underground by AngloGold Ashanti Córrego do Sítio Mineração S/A (AGA) since 2009. The deposit is hosted by the intermediate portion of the Rio das Velhas greenstone belt sequence. Sales (1998) was the first to recognize the local lithostratigraphy at the mine site. From bottom to top it is composed of metabasalt (chlorite–carbonate–sericite–quartz schists), banded chert layers with banded iron formation (BIF) that are both carbonaceous and/or ferruginous, carbonaceous and micaceous phyllites, with mineral paragenesis compatible with the greenschist facies mineralogy (Herz, 1970, 1978). Smoky quartz in silicification zones is abundant and widespread, in association with quartz veining, with these containing the highest gold grades. Replacement-style hydrothermal alteration of BIF is host to the remaining gold resources.

The deposit is structurally controlled, with veins associated with shear zones, and in accordance with rock competence, in a concordant or discordant arrangement with the foliation. Some areas have breccia textures with fragments of the host rocks. Smoky quartz veins are assigned to the first stages of mineralization, whereas milky quartz is assigned to the recrystallization of smoky quartz and/or to the final stages of the hydrothermal process (Martins, 2011). The structure at Lamego is dominated by a rootless, reclined, isoclinal fold in the sense of Ramsay (1967), called the Lamego fold (Martins et al., 2011). There are four orebodies, and these are Queimada, Carruagem, Arco da Velha and Cabeça de Pedra, the latter being the object of the present study.

The aim of this study is to contribute to the understanding of the origin, physical and chemical characteristics of the fluids and their influence on the formation of this gold deposit. At the onset we approach this objective by classifying the different vein systems of the Cabeça de Pedra orebody and detailing their petrographic characteristics. These are complemented by fluid inclusion microthermometry, arsenopyrite geothermometer and in situ LA-ICP-MS microanalyses of the fluid inclusions. Few other fluid inclusion studies have been undertaken for these deposits (e.g., Alves, 1995; Godoy, 1994; Lobato et al., 2001b; Ribeiro et al., 2015; Xavier et al., 2000), and no LA-ICP-MS microanalyses of the inclusions have even been reported. The LA-ICP-MS results from Lamego

were undertaken to demonstrate the role of the host rocks, especially carbonaceous phyllites, their influence on the source of metals and the hydrothermal fluid evolution, and were compared with results of FIs for the Carvoaria Velha gold deposit, Córrego do Sítio lineament, QF. The aims of this comparison are: i) distinguish the chemical mineralization process in two different orogenic gold deposits of the Rio das Velhas greenstone belt; and ii) establish the dominant factors defined by the fluid–rock interaction in these deposits.

2. Regional geology

The Quadrilátero Ferrífero (Fig. 1) represents a granite–gneiss terrain overlain by a greenstone-belt-type sequence of Archean age, and Proterozoic supracrustal sequences.

The granite–gneiss terrains are composed of trondhjemitic–tonalitic–granodioritic gneisses, or TTG, and represent the basement of the QF, whose most representative units are the Belo Horizonte, Bação, Caeté and Santa Barbara complexes (Fig. 1). These rocks are Paleoproterozoic to Mesoproterozoic, dated in the range 3380 to 2900 Ma (Teixeira et al., 1996), and have been subjected to metamorphism and migmatization dated between 2920–2834 Ma. They were also affected by Rhyacian (formerly Transamazonian; 2.22–2.05 Ga; Brito Neves, 2011) deformation at 2041 ± 5 Ma (Noce et al., 1998). The unit is intruded by Neoproterozoic metatonalites, metandesites, metagranites and Paleoproterozoic mafic dikes (Carneiro, 1994; Noce, 1995), and is the source of debris for the upper greenstone sedimentary units (Schrank and Machado, 1996; Schrank et al., 2002).

The Rio das Velhas greenstone belt (Fig. 1), dated in the range 2800–2740 Ma (Machado and Carneiro, 1992; Machado et al., 1989b; Noce et al., 2002, 2007), comprises a Neoproterozoic volcano–sedimentary sequence formally proposed as Rio das Velhas Supergroup by Loczy and Ladeira (1976), with two stratigraphic units, the Nova Lima and Maquiné Groups. From the base to the top, the Nova Lima Group is composed of a volcanic komatiitic–tholeiitic unit with associated chemical sedimentary rocks, superimposed by a felsic volcanoclastic unit with associated volcanism, and an upper clastic unit (Baltazar and Zucchetti, 2007). The Maquiné Group is divided into the Palmital (O'Rourke, 1957) and Casa Forte (Gair, 1962) formations. The former is composed of quartz phyllites and the latter of quartzites and conglomerates. All these rocks are metamorphosed in the greenschist facies (Herz, 1970, 1978).

The Nova Lima Group has been divided into five sedimentary lithofacies associations (Baltazar and Pedreira, 1996, 1998; Baltazar and Zucchetti, 2007; Pedreira and Silva, 1996; Zucchetti and Baltazar, 2000): mafic–ultramafic, chemical volcano–sedimentary, chemical–clastic sedimentary, volcanoclastic (where the Lamego deposit is located), resedimented (where the Carvoaria Velha deposit is located). The Maquiné Group is divided into the coastal and non-marine associations (Fig. 1).

According to Baltazar and Zucchetti (2007): (i) The mafic–ultramafic association is predominantly composed of basalts as massive and pillow flows, with minor gabbro, anorthosite and peridotite, and intercalations of BIF, ferruginous chert, carbonaceous pelite, turbidites, and rare felsic volcanoclastic rocks. (ii) The chemical volcano–sedimentary association has tholeiites intercalated with BIF and ferruginous chert, and subordinate fine-grained clastic sedimentary rocks, turbidites and pelites, intercalated with chemical rocks. (iii) The chemical–clastic sedimentary association is composed of alternating fine-grained pelites (micaceous and chloritic schists) with lesser BIF, and subordinate chert and carbonaceous schists. (iv) The volcanoclastic association has volcanoclastic felsic and mafic rocks. (v) The resedimented association comprises mainly graywackes, sandstones, and siltstones, and is widely distributed in the QF. (vi) The coastal and non-marine associations correspond to sandstone–siltstones and sandstones–conglomerates, respectively.

The Proterozoic sequences are the Minas Supergroup, Itacolomi Group and Espinhaço Supergroup. The Minas Supergroup (Dorr, 1969;

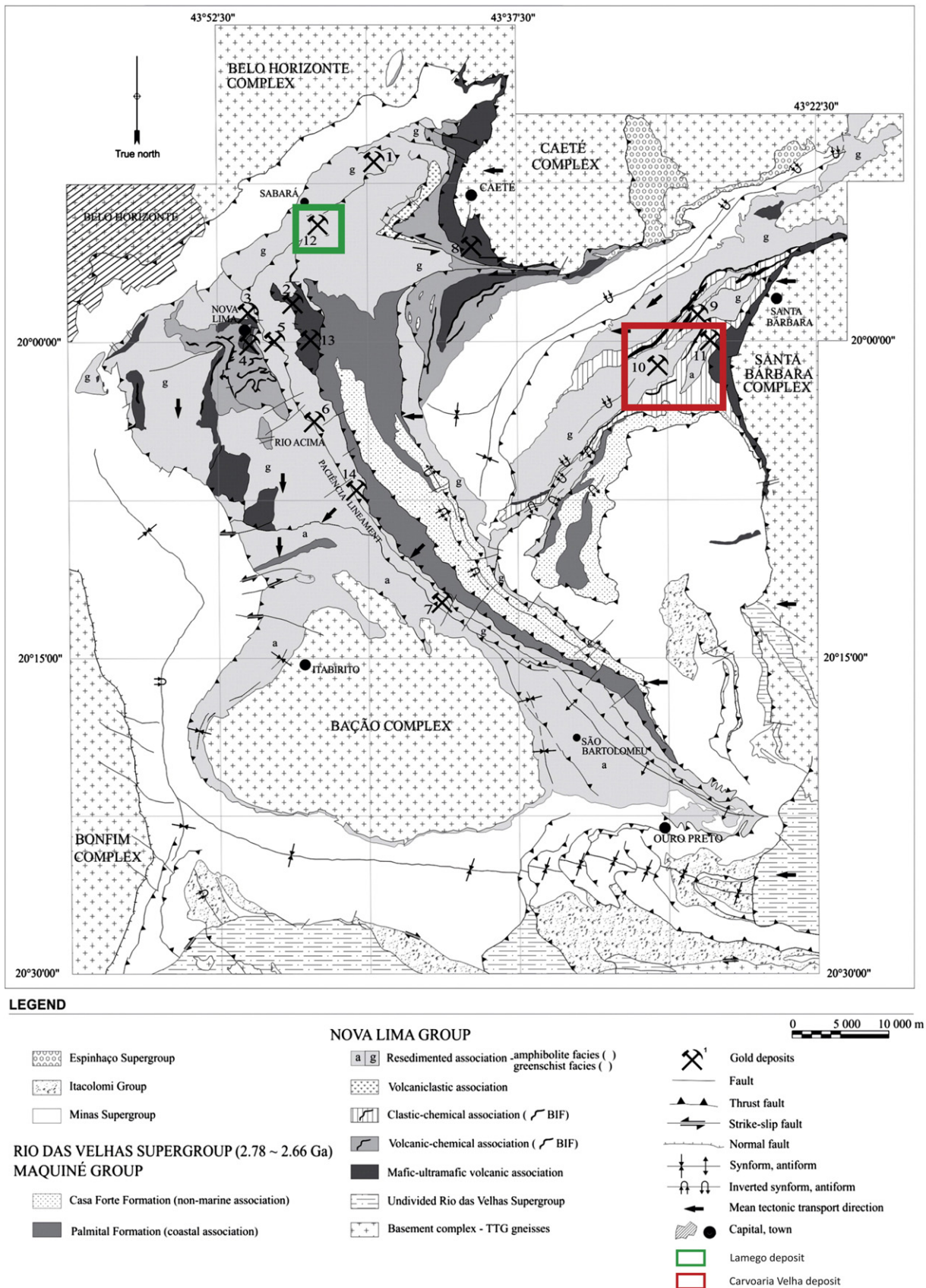


Fig. 1. Simplified geological and structural map of the Quadrilátero Ferrífero region. The main lithofacies associations of the Nova Lima Group, Rio das Velhas greenstone belt (Baltazar and Zucchetti, 2007), and some of the gold deposits are shown (from Lobato et al., 2001a, 2001b). Gold deposits: 1 – Cuiabá; 2 – Raposos; 3 – Morro Velho; 4 – Bela Fama; 5 – Bicalho; 6 – Esperança; 7 – Paciência; 8 – Juca Vieira; 9 – São Bento; 10 – Córrego do Sítio; 11 – Brumal; 12 – Lamego; 13 – Santana and 14 – Engenho d’Água. The studied area is highlighted in a green square, and detailed in Fig. 2. Also highlighted in red is the Carvoaria Velha, Córrego do Sítio lineament.

Dorr et al., 1957) is in angular and erosive discordance on the Rio das Velhas greenstone belt rocks and its distribution defines the geometric shape of the QF. It is a metasedimentary unit of Paleoproterozoic age, composed of clastic and chemical sediments hosted in a package of quartzites, metaconglomerates, metapelites and a thick sequence of iron formations of Lake Superior-type (Klein and Ladeira, 2000), which age of sedimentation had been calculated between 2580 and 2050 Ma (Renger et al., 1994).

The Itacolomi Group outcrops in the NE part of the QF and is composed of clastic sedimentary sequences. The Espinhaço Supergroup is composed of conglomerates, sandstones and mafic rocks and covers a small part of the QF that was deposited between 1840–1715 Ma (Machado et al., 1989a,b).

The structural complexity of the QF is due to the different deformational events that took place in its geological history. The controversy dealing with the subject is emphasized by the works of Belo de Oliveira and Vieira (1987), Dorr (1969), Guimarães (1931), Ladeira and Viveiros (1984), Marshak and Alkmim (1989), Oliveira et al. (1983), Vieira and Oliveira (1988), Zucchetti and Baltazar (1998).

Baltazar and Zucchetti (2007) propose four structural generations associated with three deformation events of Rio das Velhas Supergroup. The first generation D1 is associated with the Archean event, in a compressive regime, with a tectonic transport from N to S. East-striking and N-dipping thrust faults, and open, sub-horizontal flexural normal folds to S-verging and ENE-plunging tight to isoclinal folds were also characteristic. The D2 Archean event represents a compressive regime with NE to SW tectonic transport. The orientation of the thrust faults are NW (030–050/40–60), with isoclinal and tight folds having a convergence to the SW and NW directions. The stretching and mineral lineations have a (060–070/20–30) orientation. Gold mineralization in the Rio das Velhas Supergroup is assigned to this deformation event.

The D3 generation is associated with the Rhyacian-age event (2100–1900 Ma), of extensional character and tectonic transport from WNW to ESE. It is characterized by the nucleation of regional synclines and the onset of the Minas Supergroup deposition. The D4 deformation is part of the Brasiliano (650–500 Ma) tectonic cycle with compressive regime and simple shear, and convergence of E to W.

3. Local geology

3.1. Lithostratigraphy of Lamego

The Lamego deposit is in the intermediate part of the Nova Lima Group, of the volcanoclastic association of Baltazar and Zucchetti (2007). The structure at Lamego is dominated by a rootless, reclined, type-2, isoclinal fold in the sense of Ramsay (1967), called the Lamego fold (Lobato et al., 2013; Martins et al., 2011), with a 4.8 km outcropping perimeter and an axis oriented NE–SW (Martins, 2011).

The Lamego deposit (Fig. 2) has four orebodies, Queimada, in the inverted limb of the Lamego fold, Arco da Velha in the normal limb, Carruagem, where the inverted and normal limbs intercept, and Cabeça de Pedra, located in the hinge zone of the fold, and the object of study in this article.

Lamego is a BIF-hosted, orogenic-type gold deposit, which stratigraphy was initially described by Sales (1998), and re-evaluated by Martins (2011). From bottom to top, the sequence is formed by the following rocks (Fig. 2):

Metabasalt. It forms the core of the fold, and is represented by chlorite-, carbonate- and quartz-rich metabasalts. Where strongly hydrothermalized and deformed, these are chlorite–carbonate–sericite–quartz schists, that are locally sulfidized (mainly pyrite), in association with quartz veins and boudins that also contain carbonate (mainly ankerite) and sulfide minerals. The contact with

the upper units may be concordant (Martins, 2011).

Chert and BIF. This unit is formed by metamorphosed Algoma-type (Gross, 1980) BIF, and ferruginous or carbonaceous metachert. It is characterized by metachert bands associated with some very fine-grained carbonates (ankerite and siderite) and sulfide bands, composed by hydrothermal pyrite and chlorite; rare metamorphic magnetite is present. This banding is interpreted as sedimentary (Martins, 2011).

Carbonaceous phyllite. It occurs in the lower contact, normal or discordant with the BIF. It is composed mainly of carbonaceous matter, quartz, chlorite and carbonate (Martins, 2011).

Micaceous phyllite. This unit occurs on the top of the sequence, formed by quartz, carbonate, sericite–muscovite and pyrite (\pm chalcopyrite and sphalerite). The lower contact with the carbonaceous phyllite is normal and discordant (Martins, 2011).

Dolerite dikes and sills. Dolerite dikes and sills are exposed mainly in the Carruagem orebody level 1, and in the Cabeça de Pedra open pit. They may be parallel to or cross-cut both carbonaceous and micaceous pelites, and BIF. They are foliated only near the contacts with wall rocks, and contain hornblende, actinolite–tremolite, epidote, chlorite, carbonate, plagioclase, sericite and quartz (Villanova, 2011).

3.2. Lithostratigraphy of the Carvoaria Velha deposit, Córrego do Sítio lineament

The Córrego do Sítio lineament is located in the northeastern sector of the QF region (Fig. 1). The term Córrego do Sítio lineament was proposed by Lima (2012) to include several gold deposits and occurrences along a NE–SW trend, where Carvoaria Velha is located. The Carvoaria Velha orogenic gold deposit, located 130 km far from Belo Horizonte, and 120 km from the Lamego mine, is hosted in metagraywackes and carbonaceous phyllites of the Nova Lima Supergroup, and intruded by mafic dikes and sills (Roncato et al., 2015). Lithologies correspond to an alternation of metapelites and metapsamites, with gradational layering and plane-parallel and cross-bedding stratification. Subordinate thin levels of carbonaceous phyllites and BIF are present. These units are interpreted by Zucchetti and Baltazar (1998) as a result of deposition by turbidity currents. They are classified as quartz–carbonate–white mica–chlorite schists, and according to Lima (2012) represent the product of the greenschist facies metamorphism of graywackes, sandstones and carbonaceous pelites. Mafic dikes constitute tabular bodies of metric and decametric thickness, and kilometeric continuity, composed of metagabbros in different zones of hydrothermal alteration to carbonate, chlorite and sericite (Lima, 2012).

3.3. Structural geology and hydrothermal alteration at the Lamego deposit

The structural evolution at Lamego has been the object of detailed investigation by Lobato et al. (2013), Martins (2011) and Martins et al. (2011). The text that follows is a summary of their work.

The primary planar structures (S_0) are the compositional and gradational bedding that dip mainly to the SE. At levels 1 of the Queimada, Arco da Velha and Cabeça de Pedra orebodies, S_0 has an axis oriented at 117/38. The S_{1-2} foliation is the most conspicuous planar structure in the Lamego deposit, and is mostly parallel or sub-parallel to S_0 . A L_{1-2} lineation is described on the S_{1-2} foliation planes, and characterized by the intersection of this surface's planes with S_0 . For orebodies

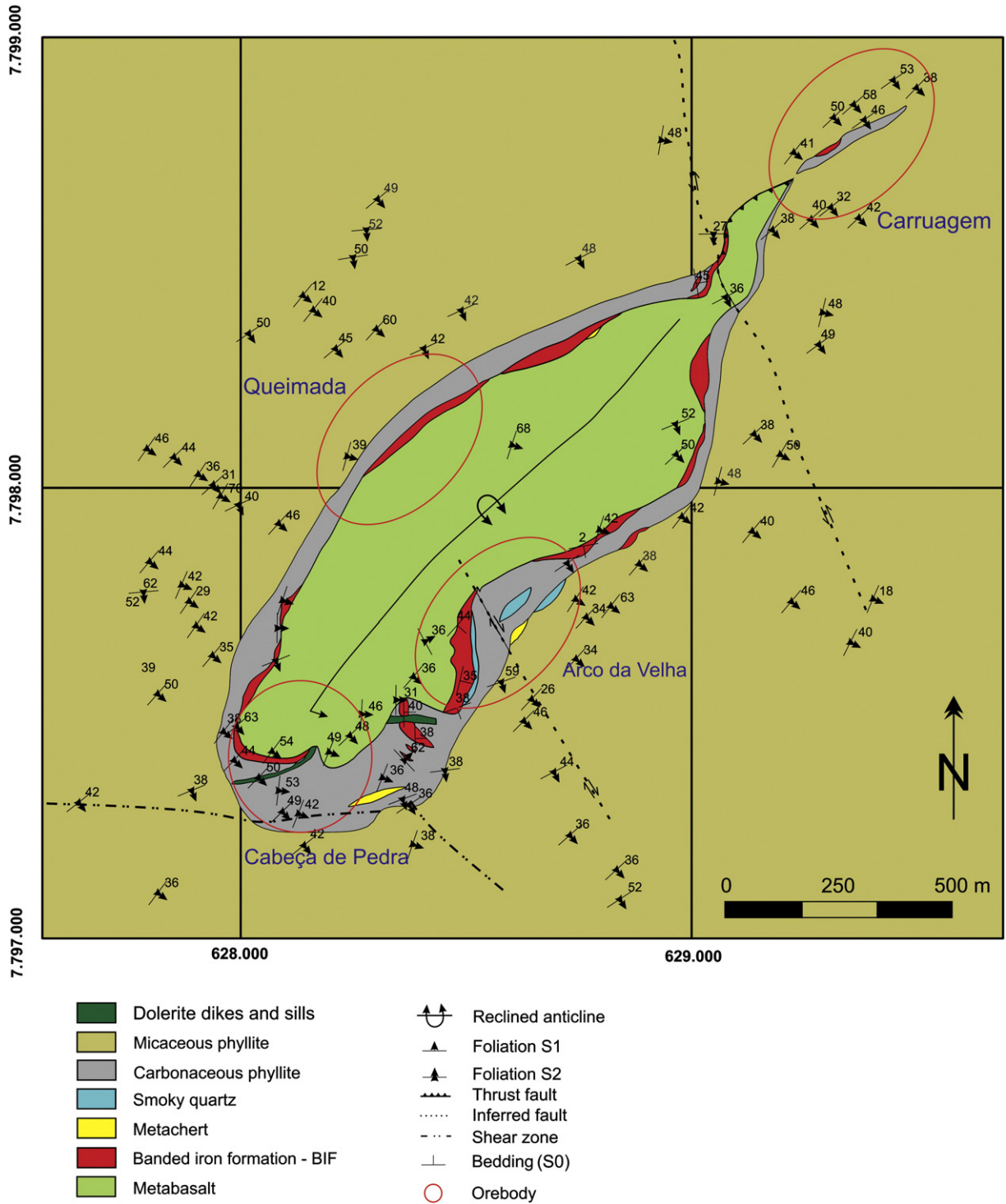


Fig. 2. Geological map of the Lamego deposit. Modified after Villanova (2011).

Queimada level 1 and Cabeça de Pedra levels 1 and 2, S_{1-2} and L_{1-2} are strongly concentrated in the SE, on average trending 124/35. Together with the bedding plane S_0 , S_{1-2} foliation defines folds that are always associated with meta-sedimentary and metavolcanic rocks. The attitude of these folds is concentrated in the SE, with a plunge close to 25°, and is parallel to sub-parallel to the mineral lineation L_{1-2} .

The S_3 crenulation cleavage, or spaced cleavage plane, is developed mainly in metapelitic rocks. The L_3 is made up by the intersection of the S_{1-2} with S_3 foliation planes. The F_3 open folds have amplitudes up to 3 m, and are best identified in the carbonaceous phyllite. The L_3 is

distributed along N–S, trends 097/85, and coincides with the S_3 foliation planes (Martins et al., 2011). Shear zones are mapped in all schistose layers and lithological contacts on centimeter to meter scale, with the development of S–C structures that indicate shearing towards the NW. Faults are restricted to the carbonaceous phyllite and dip 30° to 90°, with a consistent NW sense of reverse slip.

The structural evolution at Lamego is associated with the progressive ductile D_1 – D_2 deformation events, and D_3 that characterizes structures in a ductile–brittle environment. The orebodies have plunges varying from 95/22, in the Carruagem, to 120/25 in the Cabeça de

Pedra orebodies, respectively. The structural nature of the small orebodies that jointly comprise the four large orebodies suggests their development in a pinch-and-swell and boudin system with two orthogonal stretching directions. A chocolate-tablet structural array is thus defined during mineralization.

Hydrothermal alteration in BIF-hosted gold deposits of the Nova Lima Group are discussed by Lobato et al. (1998, 2001a), Lobato and Vieira (1998), Junqueira et al. (2007), Martins Pereira et al. (2007), Ribeiro-Rodrigues (1998), Ribeiro-Rodrigues et al. (2007), Vial et al. (2007a,b), and Vieira (1991). For the specific case of Lamego, Sales (1998) detailed the hydrothermal alteration of the mafic rocks. Lobato et al. (2013), Martins (2011), Martins et al. (2011), described significant silicification in the proximal alteration zones of ore-hosting rocks.

There are three main types of hydrothermal alteration that dominate and affect all rock types. They are represented by quartz, carbonate and sulfide minerals, and developed parallel to the S_{1-2} foliation. These alteration minerals are best exposed in BIF and carbonaceous pelites, but less well developed in the footwall metabasalt and micaceous pelites. Metabasalt is particularly altered to chlorite, sericite, carbonate, quartz, and pyrite. Widespread zones of silicification dominate, with abundant smoky and milky (recrystallization product of smoky crystals) quartz veins, and minor carbonates, sericite, pyrite and carbonaceous matter. These zones locally form breccias and boudins, with width ranging between 1 to 35 m. The sulfides are mostly represented by pyrite, As-rich pyrite, arsenopyrite, less chalcopyrite and sphalerite, and also minor pyrrhotite and galena.

4. Materials and Analytical methods

The procedures for sampling and the methods of analyses were the following:

- 1) Two drill cores (LCPD011 and LCPD009) were sampled in the Cabeça de Pedra orebody, which crosses the structure at different depths, lithologies and grades, giving priority to silicified zones (Fig. 3). Twelve polished thin sections of quartz veins were prepared for petrographic studies, and seven double polished sections (~130 μm thick) were prepared for fluid inclusions analysis.
- 2) Macro- and microscopic petrographic studies focused on quartz veins and veinlets, with definition of petrographic characteristics;
- 3) Detailed petrographic mapping of fluid inclusions (FIs) in quartz crystals from gold mineralized and barren veins was undertaken to discriminate inclusion types, sizes, morphologies and definition of fluid inclusion assemblages (FIA). A Leica petrographic microscope was used, with 10 \times oculars and objective lenses of 2.5 \times , 5 \times , 10 \times , 20 \times , 50 \times and 100 \times ;
- 4) Fluid inclusion microthermometric studies were conducted using a fully automated Linkam THMSG600 heating and freezing stage with a TMS 93 temperature controller. The stage was calibrated between $-56.6\text{ }^{\circ}\text{C}$ and $374.1\text{ }^{\circ}\text{C}$ with synthetic fluid inclusion Linkam standards (pure H_2O and mixed $\text{H}_2\text{O}-\text{CO}_2$). The cyclic technique (Goldstein and Reynolds, 1994) was used to acquire better precision in measurements of transition of temperature between carbonic

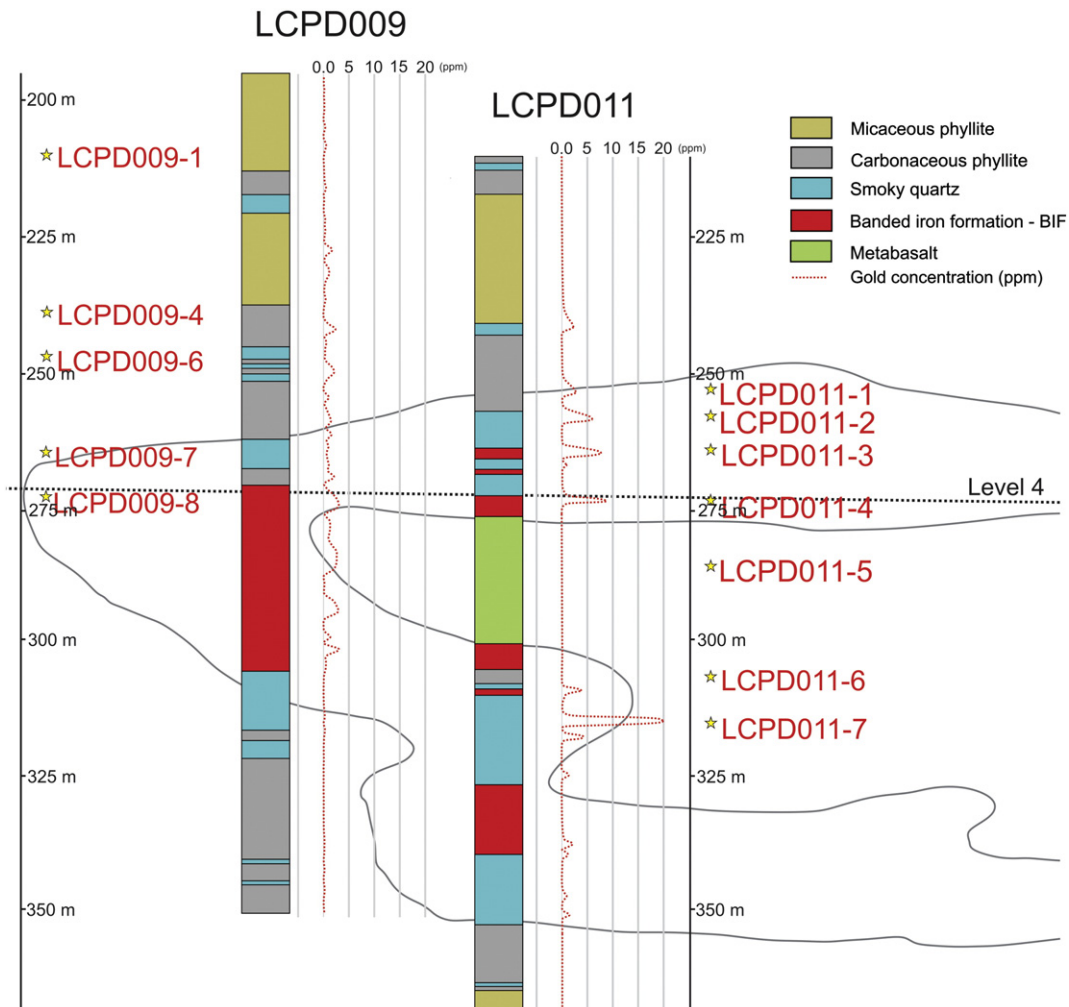


Fig. 3. Cross-section of the Cabeça de Pedra orebody, Lamego deposit, showing the schematic logging sampled LCPD009 and LCPD011 drill cores, with gold grades (in ppm) and depths from where quartz veins were collected.

phases. The accuracy of the freezing measurement runs is about ± 0.1 °C and for heating runs ± 1 °C between 200 and 500 °C. Apparent salinity has been reported in equivalent percentage weight of NaCl. Calculations of salinity and density were made using the MacFlinCor program (Brown and Hagemann, 1995);

- 5) Raman spectroscopy was used to assess gases and fluids contained within the Fls. This technique allows a correlation between the composition and phase behavior, during the studies of cooling of Fls. Raman spectra were obtained on a Jobin Yvon/Horiba LABRAM-HR 800 spectrographer equipped with a He–Ne laser (632.8 nm). The Raman signal was collected by a BX-41 Olympus microscope using 10 \times , 50 \times and 100 \times objectives. The acquisition time ranges from 10 to 120 s, depending on sample background fluorescence, and the laser power from 0.06 to 6 mW. Spectra were acquired 10–30 times to reduce signal/noise ratio. Collected Raman spectra were analyzed and optimized with Labspec 4.18 and Origin 8.0. Background was corrected and when necessary normalized and peak deconvoluted. Measurements were performed at the Raman Laboratory of Spectroscopy in the Department of Metallurgic and Materials Engineering at UFMG;
- 6) Individual inclusions were analyzed by laser-ablation inductively-coupled mass-spectrometry (LA-ICP-MS). The sections were introduced into the sample chamber of the ArF 193-nm excimer laser Geolas Q Plus. Before the chamber was closed, all air is expelled through a He flow. Inside the chamber, the samples were analyzed for 300 s, during which several inclusions were opened by the laser ablation process. The entire content of inclusions extracted is transported as an aerosol together with He gas. The samples were then analyzed by ICP-MS Agilent 7500c quadrupole, equipped with an octopole reaction cell. The analyses were calibrated using the NIST SRM 610 standard. The data collected from the ICP-MS were processed by the SILLS software (Guillong et al., 2008), for calibration, background correction and floating of the integration signal. During this procedure, to ensure that the fluid inclusion signals were being processed without the interference of the host crystal, only spectra containing signals coincident with Na and other cations were processed. This analysis was done in the Laser Ablation ICP-MS laboratory at the University of Leeds, England;
- 7) Electron microprobe analyses were performed on arsenopyrite crystals using the JEOL model JXA 8900RL, at the Electronic Microscopy and Microanalytical (LMA) Laboratory at the Physics, Geology and

Chemistry–CDTN–CNEN Consortium Laboratory, at the Universidade Federal de Minas Gerais, UFMG, Brazil.

5. Veins associated with the Cabeça de Pedra orebody

The quartz veins in the Cabeça de Pedra orebody are constrained by different structures, and are closely associated with the formation of the Lamego fold, which lithotypes control the morphology of each vein system (Table 1). Three vein systems are classified in order to study the fluid inclusions, using as a criterion the associated structures (Fig. 4). Usually, they are associated with boudins and pinch-and-swell structures, although in the more competent BIF, veins of planar features dominate. One of these systems was subsequently subdivided into four families according to the host rock type (Table 1).




The V1 veins are hinge-zone associated (Martins, 2011), crosscut all structures, and originated during the extensional phase of the Cabeça de Pedra orebody folding, with vein widths that diminish in relation to the axial fold plane. The mineralogy of V1 consists mainly of quartz, carbonate and sulfides.

As depicted in Fig. 4, where V1 veins crosscut BIF along hinge zones, the associated V1 minerals may migrate along lateral bands to form V2 veins and impose a pseudo-stratification (Fig. 4); this typically forms replacement-style sulfide mineralization. The V2 veins are usually folded and controlled by the S_{1-2} foliation or S_0 bedding plane. These veins are especially well developed in association with silicification zones along the contact between BIF and carbonaceous phyllite. Where associated with foliated rocks, such as phyllites, V2 is subdivided into V2a, V2c and V2d veins, whereas where hosted in BIF only V2b veins are defined (Fig. 4).

The V2 mineralogy is generally simple, comprising 70–80% of smoky quartz, 10–25% carbonate and 10% sulfides, in which the most common are pyrite, As-pyrite and arsenopyrite, and locally chalcopyrite and sphalerite. Arsenopyrite is especially associated with V2 veins hosted in carbonaceous phyllites (V2c). The hydrothermal alteration associated with these veins varies according to their host rock, but it is common to find chlorite and carbonates in metabasalt, carbonate and sericite in carbonaceous and micaceous phyllites, and abundant sulfides in BIF. In the silicification zones, sulfide minerals are less abundant (<5%; Martins, 2011).

The V3 veins (Table 1; Fig. 4) are classified as an independent system, once it exhibits another morphological style. It is more typical of

Table 1
Synthesis of vein characteristics in the Cabeça de Pedra orebody, Lamego deposit.

	System	Family	Host structure	Mineralogy	Host rock	Orientation	Morphology	
Mineralization grade		V1	Parallel to axial plane/hinge zone	Smoky Qtz, Py, Apy, Au	BIF	15/60	Massive/extensional veins	
		V2a	S_{1-2}	Smoky Qtz, Cb, Py, Apy, Ccp	Metabasalt	130/35	Pinch and swell, boudins	
		V2b	S_0	Smoky Qtz, Py, Apy, Au	BIF	130/35	Massive/extensional veins	
		V2	V2c	S_{1-2}	Smoky Qtz, Cb, Py, Ccp	Carbonaceous phyllite along BIF contact	130/35	Pinch and swell, boudins
			V2d	S_{1-2}	Smoky Qtz, Cb, py	Micaceous phyllite	130/35	Pinch and swell, boudins
	V3	–	–	Milky quartz veins in smoky quartz	Smoky quartz	No preferential orientation	Comb, vein arrays, tension gashes	

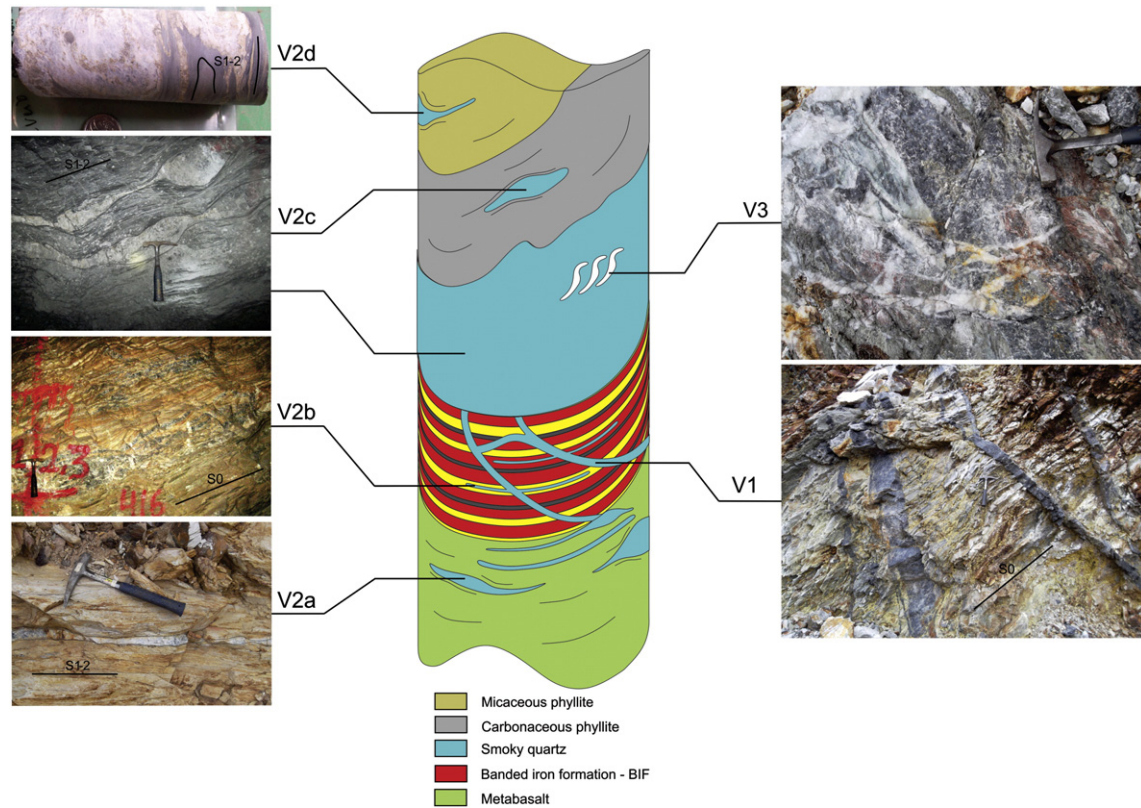


Fig. 4. Schematic diagram illustrating the different quartz vein systems at the Cabeça de Pedra orebody, Lamego deposit. Also shown are photographs of examples from core and hand samples. Veins types hosted in the metavolcano–sedimentary rocks are: V1 – smoky quartz–carbonate extensional veins that crosscut S_0 in BIF; V2a – smoky quartz–carbonate veins, along the main S_{1-2} foliation in metabasalt, which may be folded and boudinaged; V2b – smoky quartz–carbonate veins, developed along S_0 bedding plane in BIF; V2c – smoky quartz–carbonate veins, along the main S_{1-2} foliation in carbonaceous phyllite with boudins and pinch-and-swell structures, and silicification zones along the contact between BIF and carbonaceous phyllite; V2d – smoky quartz–carbonate veins controlled by S_{1-2} foliation in micaceous phyllite and V3 – milky quartz–carbonate veins in smoky quartz associated with shear zones and faults, with an echelon vein arrays and stockwork structures.

shear zones and faults, with structures like en echelon, vein arrays and stockwork, and basically consists of milky quartz veins. Comb-textured quartz crystals are also observed.

In all vein systems, quartz can be classified into two types: Qtz I – smoky, subhedral and anhedral (Fig. 5A), with medium to large grain sizes (0.5–5 mm). The Qtz I is extremely deformed, with wavy extinction, irregular, and displaying recrystallized borders. In addition, it presents a great quantity of fluid inclusions and fine fragments of carbonaceous matter. According to the mine geologists, this type of quartz carries the highest gold grades, and therefore directly associated with gold precipitation. The Qtz II is milky, granoblastic, which ranges in size from very fine (~0.05 mm) to coarse (4 mm), with the latter related to a higher degree of recrystallization (Fig. 5B). The content of carbonaceous matter, typical of the smoky quartz, decreases dramatically giving its characteristic color. This quartz is barren and interpreted as a late-stage phase.

In all mineralized veins the paragenetic sulfide sequence is pyrrhotite, pyrite, arsenical pyrite, arsenopyrite, with pyrrhotite usually as rare relicts in the nuclei of pyrite crystals. Pyrite constitutes a primary generation formed as subhedral and porous crystals, evolving to an arsenical pyrite with alteration rims (Morey et al., 2008), and finally to euhedral arsenopyrite. Gold commonly fills the porosity of arsenical pyrite (Fig. 5C).

6. Fluid inclusions

6.1. FI petrography

The fluid inclusions (FIs) were detailed according to their host minerals, mineralized (Qtz I) or barren (Qtz II), taking into account FI size, phase relations and chronological order in relation to the crystal.

Chronologically, the FI located in the center of Qtz I crystals, isolated or forming clusters, could in principal be considered as primary. However, due to the intense deformation experienced by the Lamego rocks, we adopt them as pseudosecondary and linked to gold precipitation at the early stage of hydrothermal alteration.

The FIs were grouped according to frequency, shape, relative age, size and chemical composition (acquired with Raman spectroscopy), and thus classified into five groups (Fig. 6A):

Type IA isolated clusters of pseudosecondary two-phase inclusions, at room temperature, restricted to the Qtz I, commonly with negative crystal shapes and rounded. The size ranges from < 15 μm to 5 μm , with a ratio of liquid to vapor of 9:1 (Fig. 6B).

Type IB isolated clusters of pseudosecondary two-phase inclusions, restricted to the center of the Qtz II (advanced recrystallization) crystals. The shape can be of negative crystals, and some irregular curved shapes. The size is < 20 μm to 5 μm , and the ratio of liquid to vapor is 9:1 (Fig. 6C).

Type II Trails of pseudosecondary two-phase inclusions, present in Qtz I and Qtz II, with rounded and elongated shapes (Fig. 6D). They present partial necking down. The size is < 5 μm up to 15 μm , and the ratio of liquid to vapor is 9:1. The FI are intragranular.

Type III They form linear pseudosecondary trails (Fig. 6E) aligned parallel to crystal boundaries of the Qtz II (exclusively inside polygonal granoblastic, incipient recrystallized quartz). They are enriched in liquid (< 5% vol. gas). They exhibit round shapes, are < 5 μm , which limited their analysis with the Raman spectroscopy.

Type IV Secondary inclusions crossing crystal boundaries of Qtz I and Qtz II (transgranular trails), developed late in the hydrothermal process, and strongly affected by necking down. Two-phase FIs,

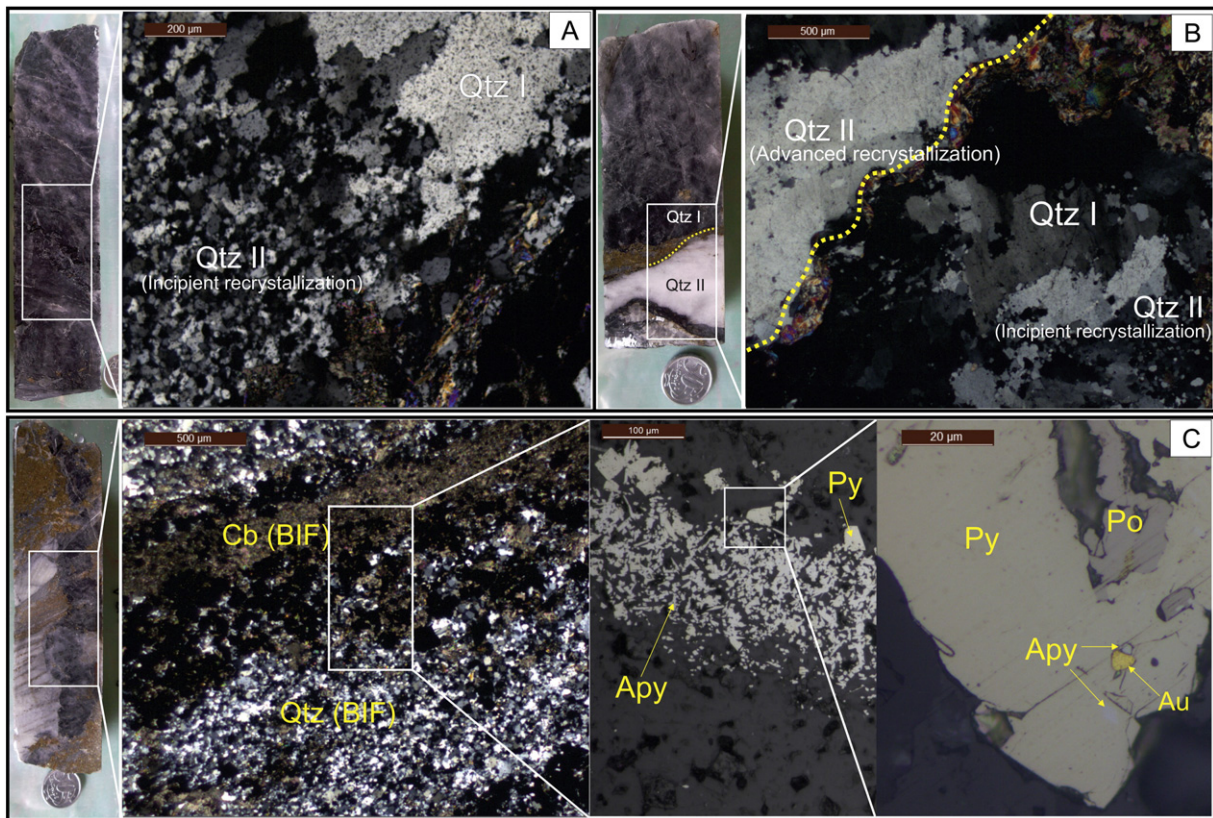


Fig. 5. Photomicrographs showing: A) Different types of quartz in V2 vein types. Qtz I is only present as smoky quartz, and Qtz II as polygonal crystals associated with Qtz I borders (transmitted light, crossed nicols, 5 \times). B) Types of quartz in V2 and V3 veins: polygonal Qtz II (incipient recrystallization) associated with Qtz I as smoky quartz, and granoblastic Qtz II (advanced recrystallization) as milky quartz (transmitted light, crossed nicols, 2.5 \times). C) Sequence of photomicrographs showing gold associated with proximal hydrothermal alteration minerals in BIF. The abbreviations correspond to: Apy – arsenopyrite; Po – pyrrhotite; Py – pyrite; Au – gold; Qtz – quartz and Cb – carbonate.

present in the two types of quartz, have irregular and amoeboid shapes. Their size ranges from <5 to 40 μm , with a liquid to vapor ratio of 9:1 (Fig. 6F).

6.2. Raman spectroscopy

The chemical composition of FIAs was determined by this technique, with the acquired spectra showing the composition without appreciable variations in the fluid evolution. All FI types (Fig. 6G) are composed by $\text{H}_2\text{O} \pm \text{CO}_2$ (wavenumber peaks of CO_2 in 1277, 37 and 1379, 36), some of them with very small proportions of CH_4 (peak in 2906, 63) and N_2 (peak in 2322, 30). The particularity of the type IA inclusions is the great amount of fine particles composed by carbonaceous matter (Fig. 6H), which are represented with the spectra of graphite with wavenumber peaks in 1329, 20 and 1578, 31 (Burke, 2001; Frezzotti et al., 2012).

6.3. Microthermometry results

Some 100 FIs were measured, and these include types IA, IB and II. The FI types III and IV were not measured due only to their minute average size of <5 μm , but also because they were strongly affected by necking down (Roedder, 1984). Results are summarized in Table 2 and Fig. 7.

6.3.1. Freezing

In Fig. 7 and Table 2, type IA, IB and II inclusions have CO_2 melting temperatures (T_{mCO_2}) ranging from -61.2 to -56.6 $^\circ\text{C}$, indicating an abundant presence of volatile CO_2 and CH_4 ratio (Shepherd et al.,

1985). These phases were confirmed by Raman spectroscopy (Fig. 6G). In relation to the temperature of the first melting ice (T_e), types IA and II inclusions range from -38.4 to -26.9 $^\circ\text{C}$, whereas type IB inclusions from -35.1 to -29.6 $^\circ\text{C}$, indicating the presence of complex cations, such as Fe^{2+} and Mg^{2+} , besides Na^+ in the fluid (Borisenko, 1977). The clathrate melting temperature (T_{Clath}) has a wide range of temperatures in type IA, with two trends between 1.9 and 5.3 $^\circ\text{C}$, and between 6.3 and 12.0 $^\circ\text{C}$ (Fig. 7). Types IB and II show a range of 1.6 to 9.5 $^\circ\text{C}$ (Fig. 7). The homogenization temperature of CO_2 (T_{hCO_2}) ranges mainly from 19 and 29 $^\circ\text{C}$ for type IA inclusions, from 18 to 25 $^\circ\text{C}$ for type IB, and 14 and 25 $^\circ\text{C}$ for type II (Fig. 7). All measured FIs homogenized to liquid.

6.3.2. Heating

All types of FIs registered decrepitation temperature (T_{dec}) prior to homogenization, with rare exceptions. The decrepitation temperature variations are between 199.5 and 365.9 $^\circ\text{C}$ in FIA IA, 220.8 $^\circ\text{C}$ and 383.3 $^\circ\text{C}$ for FIA IB, and 228.6 $^\circ\text{C}$ and 383.3 $^\circ\text{C}$ for FIA II (Table 2 and Fig. 8A, B). Few inclusions recorded total homogenization temperature (T_{htot}) to liquid within a wide range, from 185.4 to a maximum of 373.4 $^\circ\text{C}$ for all types of inclusions.

6.3.3. Quantitative estimation of fluid inclusions composition

Salinity (calculated using T_{Clath} for all inclusions), density and proportions of volatile estimates of aqueous and carbonic phases were calculated using the MacFlinCor software (Brown and Hagemann, 1995). Equations of state by Jacobs and Kerrick (1981) using the chemical system $\text{H}_2\text{O}-\text{CO}_2-\text{CH}_4-\text{NaCl}$ and Bowers and Helgeson (1983) for $\text{H}_2\text{O}-\text{CO}_2-\text{NaCl}$ were applied for all FI types. Fluid inclusions containing CH_4 ratios of the volatile phase were calculated using the graphical method by Thiéry et al. (1994). The salinity values and

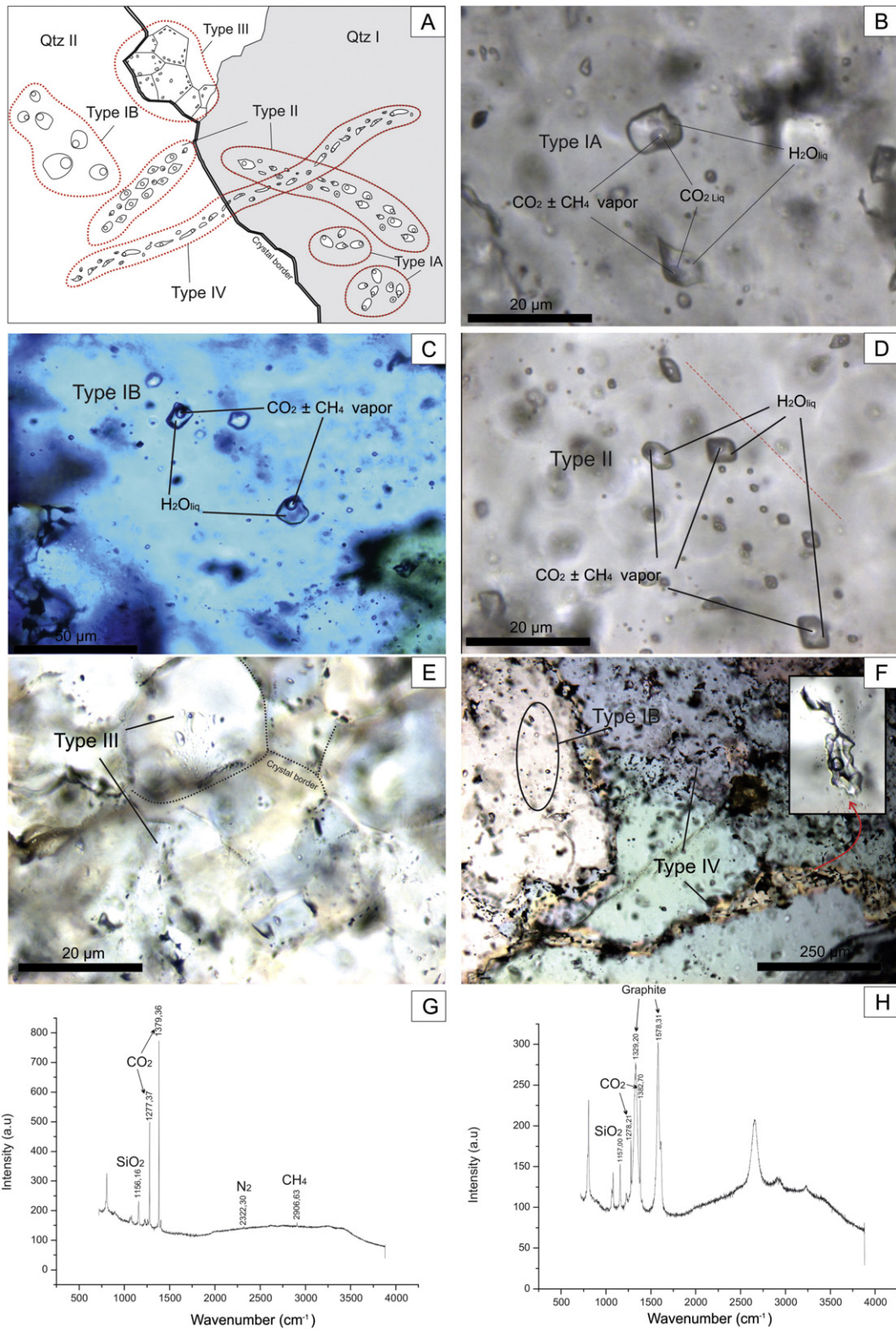


Fig. 6. A) Schematic map showing the distribution (at room temperature) of the main fluid inclusion types in mineralized and barren quartz veins at the Cabeça de Pedra orebody, Lamego deposit. Photomicrographs showing: B) pseudosecondary type IA inclusions (square, rectangular or oval in shape) restricted to smoky quartz (Qtz I); C) pseudosecondary type IB inclusions restricted to recrystallized quartz (advanced Qtz II); D) pseudosecondary trails of type II inclusions in Qtz I; E) clusters of pseudosecondary aqueous type III inclusions associated with recrystallized quartz (incipient Qtz II) and F) trails of secondary type IV fluid inclusions with necking down. G) Representative Raman spectra of all types of fluid inclusion with more abundant components in the vapor phase. H) Raman spectra of a type IA fluid inclusion with graphite fragments.

density vary widely, 0.02 to 13.32 eq. wt.% NaCl and 0.91 to 1.07 g/cm³ for type IA, 6.3 to 11.88 eq. wt.% NaCl and 0.98 to 1.06 g/cm³ for type IB and 1.02 to 13.69 eq. wt.% NaCl and 0.91 to

1.01 g/cm³ for type II (Table 3 and Fig. 8F). In relation to the carbonic phase, all FIs contain values from 1 to 8 mol% CO₂, and a maximum of 1.7 mol% CH₄ (Table 3).

Table 2
Microthermometry data for V1, V2 and V3 veins of the Cabeça de Pedra Orebody, Lamego deposit. Mean and standard deviation (1σ) values are shown for $N > 3$ in the second line of each sample.

Sample	Vein type	FI type	N	T_{mCO_2}	T_e	T_{Clath}	T_{hCO_2}	T_o	$T_{hot\ L-V}$	T_{Dec}
11-3	V2	IA	6	-59.9 to -56.6	-35.8 to -31.2	6.3 to 9.7	22.4 to 28	L	-	211.8 to 259.2
				-58 ± 1.41	-33.725 ± 1.92	8.38 ± 1.52	25.05 ± 2.35			240.93 ± 17.75
11-3	V2	II	6	-58.8 to -56.8	-32.3 to -28.3	3.1 to 8.6	15.5 to 27.7	L	366.5	253.8 to 297.4
				-57.65 ± 0.75	-30.78 ± 1.41	6.22 ± 1.97	20.42 ± 5.39			278.27 ± 21.71
9-7	V2	IA	4	-58.1 to -56.6	-35.5 to -30.4	1.9 to 2.8	23.8 to 28.8	L	-	230.7 to 234.1
				-57.4 ± 0.61	-32.97 ± 2.69	2.4 ± 0.42	25.525 ± 2.20			232.77 ± 1.64
11-2	V2	IA	9	-59.2 to -57.1	-36.7 to -29.5	2.4 to 5.3	21.8 to 29.3	L	-	174.8 to 296.4
				-57.9 ± 0.80	-32.51 ± 2.23	3.9 ± 0.90	25.14 ± 2.36			243.85 ± 43.45
11-7	V2	IA	3	-61.2 to -57.9	-36.2 to -29.8	3.1 to 4.9	5.5 to 9.3	L	-	283 to 290.5
				-59.2 ± 1.72	-32.7 ± 3.24	4.16 ± 0.94	7.83 ± 2.04			286.75 ± 5.30
9-8	V1	IA	10	-59.8 to -57.0	-38.4 to -31.6	7.8 to 10	14.4 to 29	L	272.65	199.5 to 365.9
				-58.2 ± 0.97	-34.93 ± 2.27	9.07 ± 0.71	22.36 ± 4.12			272.63 ± 44.79
9-7	V3	IB	7	-57.2 to -56.6	-34.7 to -29.6	3.4 to 4.8	17.1 to 24.5	L	185.4	242.1 to 300
				-56.82 ± 0.24	-32.54 ± 2.01	3.92 ± 0.54	21.31 ± 2.39			266.58 ± 19.19
11-2	V3	IB	12	-59.4 to -56.6	-35.1 to -31.3	3.6 to 5.1	19.9 to 25.8	L	232.8	234.5 to 260.3
				-57.48 ± 0.82	-33.82 ± 1.25	4.44 ± 0.51	23.46 ± 2.09			243.94 ± 7.39
11-5	V3	IB	2	-58.1 to -59.6	-32.5 to -31.4	6.5 to 6.6	18.2 to 23.4	L	-	284.6 to 293.7
9-6	V3	IB	9	-57.9 to -56.6	-34.6 to -31.9	3 to 5.8	15.4 to 23.1	L	223.9 to 319.6	220.8 to 383.3
				-57.02 ± 0.40	-33.7 ± 0.99	4.5 ± 1.01	20.04 ± 2.54		259.53 ± 52.31	291.02 ± 56.94
9-7	V3	II	9	-60.2 to -57.2	-36.6 to -26.9	4.3 to 5.7	13.6 to 21.9	L	314.4	264.7 to 295.5
				-58.53 ± 1.06	-31.32 ± 3.52	4.86 ± 0.44	17.25 ± 2.59			278.11 ± 11.34
11-2	V3	II	8	-58.9 to -56.6	-33.2 to -29.8	1.6 to 5.3	14.2 to 25.8	L	319.9	248.9 to 269.3
				-57.32 ± 0.84	-31.55 ± 1.21	4.23 ± 1.57	20.91 ± 4.00			258.34 ± 8.11
11-5	V3	II	4	-58.1 to -56.6	-33.3 to -28.2	6.8 to 9.5	18.3 to 28.8	L	373.4	228.6 to 274.9
				-57.32 ± 0.78	-30.5 ± 2.58	7.77 ± 1.18	23.37 ± 4.35			246.4 ± 24.93
9-6	V3	II	9	-60.2 to -56.8	-33.5 to -29.7	3.6 to 5.8	17.8 to 25.2	L	318.9	233.4 to 331.2
				-57.98 ± 1.05	-31.41 ± 1.33	4.755 ± 0.79	20.02 ± 2.41			264.73 ± 29.88

Abbreviations: T_{mCO_2} – melting temperature of CO_2 , T_{Clath} – clathrate melting temperature, T_{hCO_2} – CO_2 homogenization temperature with transition from liquid to gas, $T_{hot\ L-V}$ – total homogenization temperature from liquid to vapor phase, T_{Dec} – decrepitation temperature and T_e – eutectic temperature. N – measurement value. – Not registered.

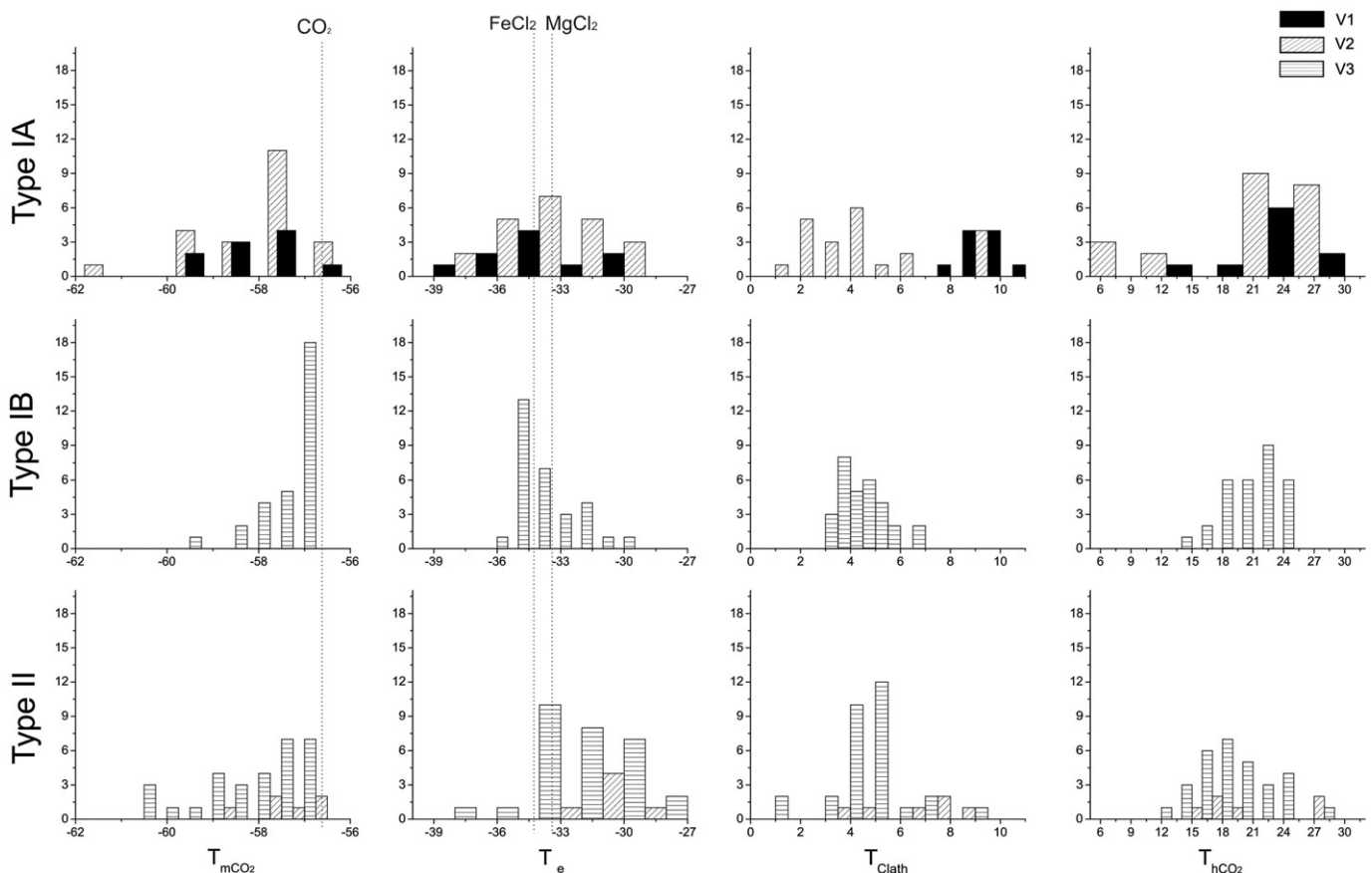


Fig. 7. Histograms showing microthermometric characteristics of fluid inclusions trapped in quartz veins from the Cabeça de Pedra orebody, Lamego deposit. Microthermometry data include CO_2 melting (T_{mCO_2}), first melting ice (T_e), clathrate melting (T_{mCl}), and CO_2 homogenization (T_{hCO_2}) temperatures.

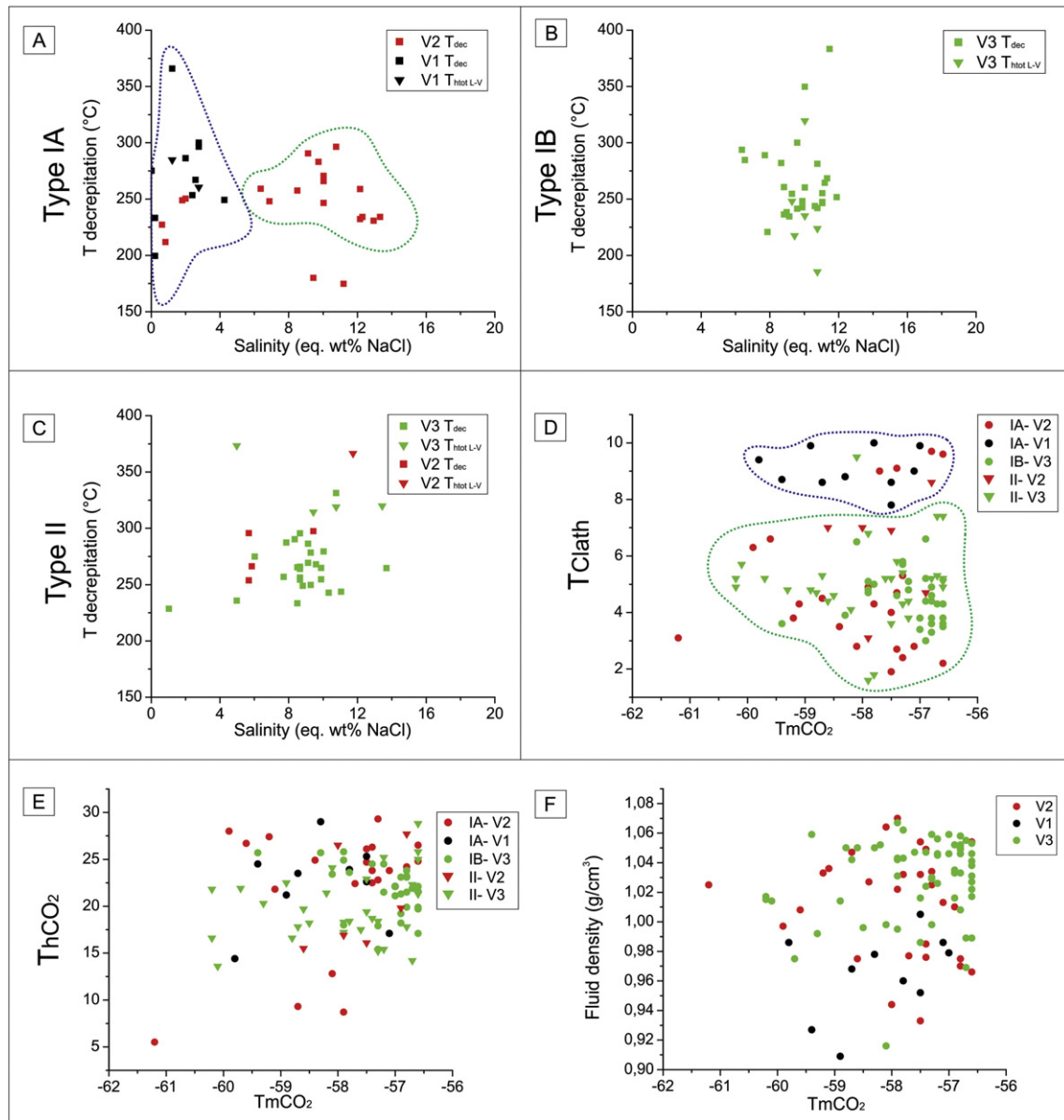


Fig. 8. Diagrams showing salinity versus decrepitation (T_{dec}) temperature for inclusions: A) type IA; B) type IB; C) type II with a few data of total homogenization ($T_{hot L-V}$). See the different populations of inclusions. D) Diagram showing content of CH_4 (determined with T_{mCO_2}) vs T_{Clath} . Note the dispersion data and two different populations defined for salinity in each vein system. E) Diagram T_{mCO_2} vs T_{hCO_2} . The dispersion data indicate the same CH_4 content in all vein systems and similar characteristics of CO_2 density. F) T_{mCO_2} vs fluid density diagram illustrating a higher density for the V3 veins. This is caused by the major concentration of NaCl in the V3 veins with low CH_4 concentration. On the other hand, V1 veins have lower densities although this is not related to the CH_4 content.

7. LA-ICP-MS fluid inclusion analyses

7.1. Cabeça de Pedra orebody, Lamego deposit

Individual measurements of the elements K, Ca, Mg, Mn, Fe, Cu, Zn, Sr, Ag, Ba, La, Pb, Li, As, Sb and Au were made using LA-ICP-MS at least in 230 FIs of types (Fig. 9 and Table 4): (i) IA in samples 9-8 (V1 vein hosted in BIF), 11-3 (V2 vein hosted in BIF) and 11-7 (V2 vein hosted in carbonaceous phyllites); and (ii) IB in samples 9-7 and 11-2 (V3 vein hosted in carbonaceous phyllites). Lanthanum was discarded as concentrations represent interference of host mineral (matrix); concentrations of Li are below detection (LOD) in all analyses, as well as the majority of Au and Ag measurements. In the case of Au and As, they were measured separately or were not measured for every inclusion assemblage, as is the case of sample 11-7.

Fig. 9 and Table 4 show that the concentration of the cations Na, K, Ca and Mg increases proportionately to salinity in all vein types, and all

analyzed inclusions are Na rich. Manganese is found at low levels and Fe concentration is maintained without a significant change in all types of veins (Fig. 9). The base metals Cu, Zn and Pb increase in their concentration in quartz veins hosted in carbonaceous phyllites, as well as Sr, in comparison to veins hosted in BIF (Fig. 9), where the concentrations of these elements are considerably lower. The metals Ag, Sb, As and Au have low concentrations in the measured fluid inclusions in all vein types, with some increase in content, especially Sb and As, in veins hosted in carbonaceous phyllites (Fig. 9).

7.2. Carvoaria Velha deposit, Córrego do Sítio lineament

According to Ribeiro et al. (2015), quartz veins associated with mineralization are V1 system (see Table 5), composed mainly of quartz and carbonate, and contain FIs classified as types 1A and 1B. Type 1A inclusions are pseudosecondary trapped in smoky quartz (Qtz 1) with a composition of $H_2O + CO_2 \pm CH_4$, salinity in the range of 4.7 to 13.2 eq. wt.%

Table 3
Microthermometric data of aqueous–carbonic inclusions (types IA, IB and II).

Sample	Vein type	FI type	N	Eq. wt.% NaCl	Bulk XH ₂ O	Bulk XCO ₂	Bulk XNaCl	Bulk XCH ₄	Bulk density	Bulk molar volume
11-3	V2	IA	6	0.63 to 6.87	0.94 to 0.97	0.02 to 0.033	0.002 to 0.021	0 to 0.003	0.966 to 1.01	19.50 to 19.62
				3.08 ± 2.79	0.95 ± 0.01	0.09 ± 0.003	0.01 ± 0.01	0.001 ± 0.001	0.98 ± 0.01	19.55 ± 0.04
11-3	V2	II	6	2.76 to 11.75	0.81 to 0.96	0.02 to 0.17	0.008 to 0.039	0 to 0.06	0.93 to 1.07	18.70 to 24.85
				6.86 ± 3.19	0.91 ± 0.05	0.07 ± 0.05	0.02 ± 0.01	0.003 ± 0.002	0.98 ± 0.05	21.07 ± 2.10
9-7	V2	IA	4	12.15 to 13.32	0.92 to 0.93	0.029 to 0.03	0.04 to 0.04	0 to 0.02	1.04 to 1.06	19.31 to 19.52
				12.67 ± 0.55	0.92 ± 0.002	0.031 ± 0.002	0.041 ± 0.002	0.001 ± 0.001	1.05 ± 0.006	19.45 ± 0.09
11-2	V2	IA	9	8.50 to 12.68	0.89 to 0.94	0.02 to 0.07	0.02 to 0.04	0 to 0.002	0.98 to 1.04	19.45 to 21.18
				10.53 ± 1.31	0.93 ± 0.01	0.03 ± 0.016	0.033 ± 0.004	0.001 ± 0.001	1.02 ± 0.02	19.88 ± 0.71
11-7	V2	IA	3	9.12 to 11.74	0.89 to 0.93	0.033 to 0.075	0.03 to 0.04	0.003 to 0.01	1.022 to 1.047	19.29 to 20.85
				10.20 ± 1.37	0.91 ± 0.02	0.05 ± 0.02	0.032 ± 0.005	0.006 ± 0.003	1.03 ± 0.014	20.29 ± 0.87
9-8	V1	IA	10	0.02 to 4.25	0.92 to 0.98	0.013 to 0.066	0 to 0.013	0 to 0.007	0.91 to 1.005	18.81 to 21.45
				1.84 ± 1.39	0.95 ± 0.019	0.032 ± 0.017	0.006 ± 0.004	0.003 ± 0.003	0.97 ± 0.029	19.86 ± 1.05
9-7	V3	IB	7	9.28 to 11.33	0.89 to 0.95	0.015 to 0.074	0.03 to 0.04	0 to 0.001	1.01 to 1.06	18.75 to 20.92
				10.56 ± 0.81	0.93 ± 0.02	0.036 ± 0.018	0.03 ± 0.003	0.0003 ± 0.0005	1.041 ± 0.015	19.55 ± 0.66
11-2	V3	IB	12	8.82 to 11.05	0.93 to 0.96	0.012 to 0.034	0.028 to 0.036	0 to 0.001	1.03 to 1.059	18.73 to 19.46
				9.81 ± 0.76	0.94 ± 0.009	0.019 ± 0.008	0.031 ± 0.003	0.0002 ± 0.0004	1.04 ± 0.006	18.93 ± 0.29
11-5	V3	IB	2	6.37 to 6.54	0.94 to 0.95	0.025 to 0.034	0.02 to 0.021	0	0.998 to 1.016	19.39 to 19.58
				7.70 to 11.88	0.90 to 0.95	0.015 to 0.072	0.023 to 0.039	0 to 0.009	0.91 to 1.06	18.73 to 20.91
9-6	V3	IB	9	9.69 ± 1.51	0.935 ± 0.014	0.03 ± 0.02	0.031 ± 0.005	0.003 ± 0.003	1.038 ± 0.018	19.43 ± 0.62
				7.86 to 10.03	0.90 to 0.95	0.014 to 0.06	0.025 to 0.033	0 to 0.009	0.97 to 1.05	18.67 to 21.22
11-2	V3	II	9	9.17 ± 0.68	0.93 ± 0.021	0.03 ± 0.020	0.029 ± 0.0025	0.003 ± 0.003	1.021 ± 0.029	19.75 ± 1.07
				8.50 to 13.69	0.79 to 0.95	0.023 to 0.18	0.023 to 0.045	0 to 0.002	0.96 to 1.07	19.40 to 24.51
11-5	V3	II	4	10.02 ± 2.20	0.91 ± 0.05	0.053 ± 0.054	0.032 ± 0.008	0.001 ± 0.001	1.022 ± 0.33	20.31 ± 1.79
				1.02 to 6.03	0.93 to 0.96	0.028 to 0.053	0.003 to 0.018	0 to 0.004	0.92 to 1.01	20.19 to 21.42
9-6	V3	II	9	4.25 ± 2.21	0.94 ± 0.016	0.045 ± 0.012	0.013 ± 0.007	0.006 ± 0.002	0.97 ± 0.037	20.35 ± 0.77
				7.70 to 11.05	0.89 to 0.96	0.013 to 0.075	0.024 to 0.035	0 to 0.004	1.008 to 1.057	18.72 to 20.95
9-6	V3	II	9	9.32 ± 1.20	0.93 ± 0.02	0.032 ± 0.024	0.029 ± 0.004	0.001 ± 0.001	1.03 ± 0.18	19.47 ± 0.88

NaCl, and a density of 0.94 to 1.06 g/cm³. Type 1B inclusions are pseudosecondary, restricted to recrystallized quartz (Qtz II), characterized by H₂O + CO₂ ± CH₄ composition and density of 0.92 to 1.04 g/cm³. The V4 veins are hosted in mafic dikes (generation DB1), and contain pseudosecondary aqueous fluid inclusions classified as type 2, with an average salinity of 15 eq. wt.% NaCl, and density between 0.97 and 0.99 g/cm³.

In the present work, about 125 individual FIs of types 1A, 1B and 2 of Ribeiro et al. (2015) were measured for comparison, using in situ LA-ICP-MS. They correspond to samples 192.2 and 195.7, which include V1 veins hosted in carbonaceous phyllite; 130.0 where a V1 vein is hosted in metagraywacke, and 160.0 with a V4 vein hosted in mafic dike – DB1, dominated by chlorite and carbonate alteration, with subordinate pyrite and quartz.

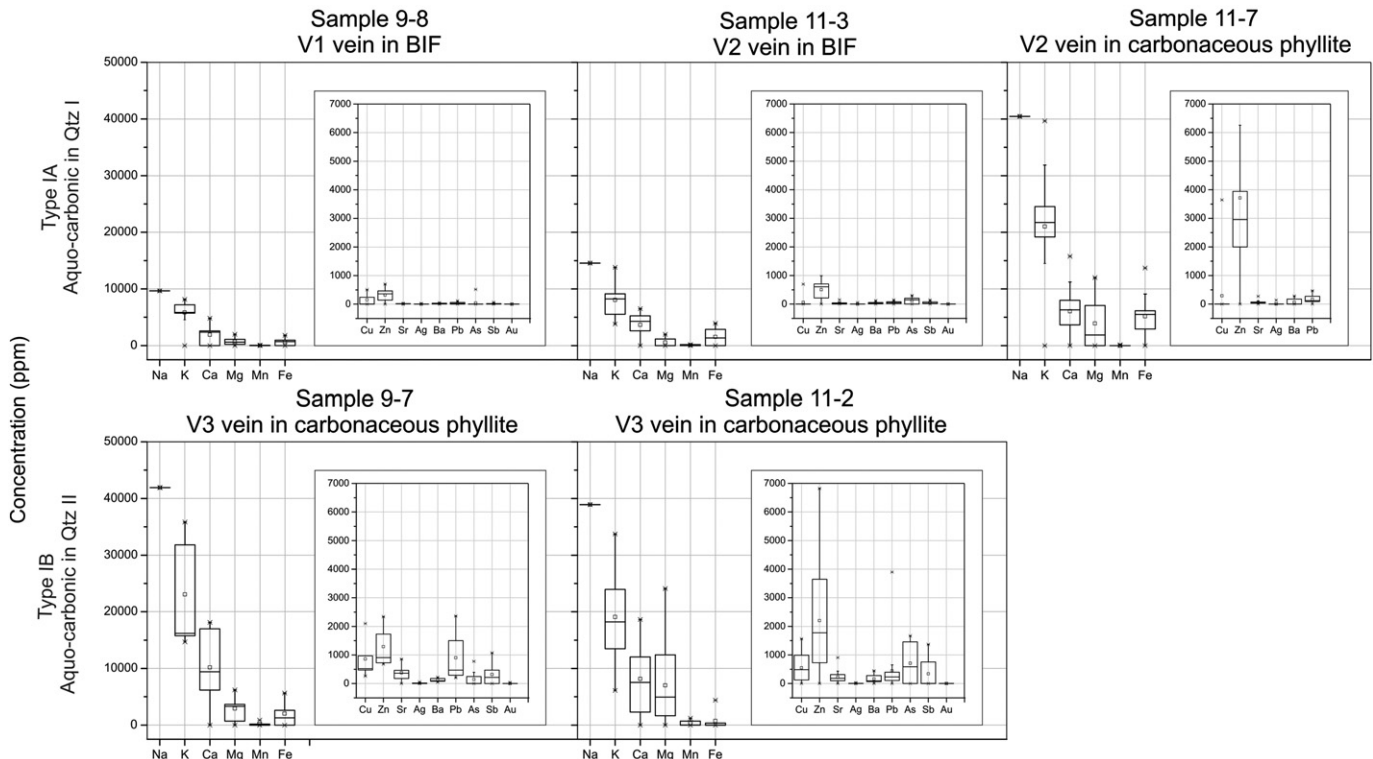


Fig. 9. Diagrams showing metal concentrations obtained from the LA-ICP-MS microanalyses of fluid inclusion assemblages and individual fluid inclusions in the Cabeça de Pedra orebody, Lamego deposit. The box plot represents the average value for a fluid inclusion type, with the respective standard deviations shown by the error bars in different vein types.

Table 4

Summary of LA-ICP-MS analyses of FI in the Cabeça de Pedra orebody. Individual element concentrations are in ppm, calculated using the salinity of the fluid inclusions.

Sample	FI type	N FI	Salinity (wt.%)	Na	K	Ca	Mg	Mn	Fe	Cu	Zn	Sr	Ag	Ba	Pb	Li	N FI	As	Ag	Sb	Au
9-8	IA	10	2.43	9656	5656	1984	598	32	845	151	321	17	3	9	40	–	13	37	1	12	–
	IA	9	2.43	9656	6741	1573	520	–	416	40	302	13	2	20	29	–	14	46	–	22	3
	IA	8	2.43	9656	6143	1673	820	8	443	201	304	12	4	22	25	–	–	–	–	–	–
11-3	IA	6	3.67	14,571	10,249	1917	432	55	1178	174	359	46	2	74	86	–	10	183	1	43	–
	IA	7	3.67	14,571	7078	4324	434	135	1934	–	575	31	1	15	45	–	12	133	1	43	2
11-7	IA	5	3.67	14,571	6201	5426	995	–	1211	–	612	22	8	47	49	–	11	65	8	58	–
	IA	6	10.2	40,465	21,164	4621	5359	–	5385	–	3783	42	–	53	59	–	–	–	–	–	–
	IA	9	10.2	40,465	21,811	5718	4457	–	4888	–	3252	65	–	95	179	–	–	–	–	–	–
	IA	11	10.2	40,465	22,923	5730	4018	–	3212	818	3482	47	20	36	179	–	–	–	–	–	–
9-7	IA	7	10.2	40,465	23,114	8019	431	–	5940	433	2179	53	–	29	267	–	–	–	–	–	–
	IA	6	10.2	40,465	25,006	3818	3862	36	4953	–	2490	44	–	120	135	–	–	–	–	–	–
	IB	7	10.56	41,907	19,363	13,211	4875	–	2567	368	793	232	4	111	384	–	13	39	12	244	–
	IB	9	10.56	41,907	31,796	6189	716	–	1294	527	726	363	50	44	202	–	15	229	12	378	41
11-2	IB	5	10.56	41,907	22,600	9502	2330	351	1891	1293	1819	478	–	159	1482	–	–	–	–	–	–
	IB	7	9.81	38,914	20,541	8262	4682	207	1026	446	2433	336	5	191	785	–	13	975	–	372	–
	IB	8	9.81	38,914	15,735	4802	12,994	534	920	796	2597	103	4	195	236	–	7	–	–	254	–
	IB	6	9.81	38,914	21,734	12,729	1916	230	74	350	1316	246	2	60	257	–	–	–	–	–	–

Note: – = below detection limit or not measured.

The results (Table 6 and Fig. 10) indicate higher contents of the cations $Na > K > Ca > Mg$ in V1 veins hosted in carbonaceous phyllite and metagraywacke, increasing their concentration as a function of salinity. In the case of the V4 veins, the concentration of these elements is higher due to their significantly greater salinity, but also the Ca and Mg concentration increases in comparison to K. There is a noticeable difference in the contents of base metals, which have a higher concentration in V4 veins hosted in mafic dikes, mainly Cu and Zn, and also Sr and Ba. In V1 veins hosted in both carbonaceous phyllite and metagraywacke, there is a positive Zn:Cu ratio (Fig. 10). The Cu:Zn ratio is positive in V4 veins for mafic rocks (Fig. 10). Another important observation is the high Sb concentration in the V1 veins hosted in carbonaceous phyllite, with a moderate concentration of As, in contrast with V1 vein hosted in metagraywacke, which is more depleted in both metals. For the case of Au and Ag, these are usually below the detection limit in all veins. Lithium is also below the detection limit.

8. Arsenopyrite geothermometer and pressure estimation for the Cabeça de Pedra orebody, Lamego deposit

Arsenopyrite may be used as a geothermometer when the variation of the arsenic content in the ore is equivalent to the temperature of formation, by using the phase diagram of the Fe–As–S system (Kretschmar and Scott, 1976). According to the authors, some criteria must be considered, and these include mineral paragenesis in the Fe–As–S system; application to ore systems where arsenopyrite formed at temperatures >300 °C; and concentration of elements as Ni, Co and Sb less than 1 wt.%.

For the case of the Cabeça de Pedra orebody, the chemical composition of arsenopyrite crystals was measured in samples 11-3a, 11-3b, 11-4 and 11-5, where crystals are in equilibrium with gold particles,

and with parageneses matching the Apy–Py stability field (Fig. 11B). Arsenopyrite crystals are commonly associated with the alteration rims of As-rich pyrite, where some crystal areas are more enriched in arsenic than others (Fig. 11A), the former being associated with gold precipitation (Morey et al., 2008). The results of the microprobe analyses are shown in Table 7, the atomic percentage of As being between 28.17 and 30.61 at%, with an average of 29.83 at%. Using the diagram proposed by Kretschmar and Scott (1976), temperatures of formation equivalent to atomic percentages of As are in the range of 300 to 375 °C, and an average of 337.5 °C (Fig. 11B).

The pressure estimates for the Cabeça de Pedra orebody were calculated intercepting the temperature of the arsenopyrite geothermometer. This is designed vertically with the fluid inclusion isochores of $H_2O + CO_2$ and $H_2O + CO_2 \pm CH_4$ systems, assuming that the inclusions were not affected by any other processes after trapping (Brown and Hagemann, 1995; Hagemann, 1993). The results for low salinity FIs (~2 eq. wt.% NaCl; see Fig. 11C) indicate a minimum pressure of 2659 bar for the $H_2O + CO_2 \pm CH_4$ system, and 2814 bar for the $H_2O + CO_2$ system. For FIs with moderate salinity (~9 eq. wt.% NaCl), pressure values are higher than 3.5 kbar (Fig. 11C).

9. Discussion

9.1. Nature of veins in the Cabeça de Pedra orebody

Quartz veins are classified according to their structural characteristics, mineralogy and field crosscutting relationships, in order to establish the chronological sequence presented in Fig. 4. The V1 vein system is hinge-zone associated, crosscut all structures, and originated during the extensional phase of the Cabeça de Pedra orebody folding. During folding, competent rocks, such as BIF, fractured parallel to the

Table 5

Synthesis of vein characteristics in the Carvoaria Velha deposit. From Ribeiro et al. (2015).

Type	Mineralogy	Thickness	Host rock	Geometry	Orientation	Distribution and nature
Related to mineralization	V1 Quartz–ankerite–sulfides/sulfosalt–gold veins	1–600 cm	Metagraywacke, schist and phyllite	• Lenticular in schistosity • Millimetric to centimetric folded veinlets • Pinch-and-swell	118/70	• Parallel to schistosity to Sn • Folded with axial plane foliation • Shear veins
Late to mineralized veins	V2 Quartz–ankerite–pyrite veins	2–300 cm	Metagraywacke, schist and phyllite	• Lenticular centimetric and metric veins	286/33	• Parallel to schistosity Sn + 1 • Extensional veins
	V3 Quartz–ankerite veins	1–20 cm	Metagraywacke, schist and phyllite	• Planar to fracture arrays, brecciated	054/84	• Parallel to schistosity Sn + 3 • Fracture veins
	V4 Quartz–calcite veins	1–15 cm	Metamafic dykes and sills	• Irregular to stockwork		• Irregular • Extensional veins

Table 6
Summary of LA-ICP-MS analyses of FI in the Carvoaria Velha, Córrego do Sitio deposit. Individual element concentrations are in ppm, calculated using the salinity of the fluid inclusions.

Sample	FI type	N FI	Salinity (wt.%)	Na	K	Ca	Mg	Mn	Fe	Cu	Zn	Sr	Ag	Ba	Pb	Li
192.2	IA	10	8.6	34,099	20,626	4974	1665	1027	4312	583	435	30	11	157	280	–
195.7	IA	4	5.8	22,997	15,460	3169	330	–	1859	1311	376	55	38	186	213	–
130.0	IB	8	4.5	17,843	12,153	1990	954	20	1866	230	390	79	8	49	103	–
	IB	5	4.5	17,843	11,300	3588	892	26	1362	314	214	59	9	35	44	–
	IB	8	4.5	17,843	12,681	1609	795	71	1628	465	449	38	1	28	78	–
195.7	IB	8	8.5	33,703	23,195	3753	1473	1105	1763	795	804	191	57	319	247	–
	IB	9	8.5	33,703	19,866	1756	4709	167	5180	502	782	180	45	241	275	–
160.0	II	6	15	59,475	24,271	20,736	7504	2620	2249	3421	430	545	17	404	98	–
	II	7	15	59,475	43,444	–	10,018	4519	–	2344	299	306	79	368	108	–

Sample	FI type	N FI	Salinity (wt.%)	As	Ag	Sb	Au
192.2	IA	10	8.6	141.6	5.1	1851.1	0.4
	IA	8	8.6	36.1	6.5	975.4	1.0
	IA	5	8.6	–	6.0	6888.1	–
	IA	2	8.6	575.7	18.3	12,407.9	7.5
	IA	8	8.6	790.0	23.3	7311.5	4.3
130.0	IB	7	4.5	45.2	10.9	82.9	–
	IB	6	4.5	162.8	8.4	3172.7	–
	IB	6	4.5	67.3	15.1	102.8	–
195.7	IB	4	8.5	1057.4	50.3	3292.8	85.8
	IB	4	8.5	2474.0	38.9	2866.0	47.4

Note: – = below detection limit or not measured.

axis near the hinge zone, allowing fluid to infiltrate via faults and shear zones (Martins et al., 2011) that acted as channels and created the V1 vein system, dominated by smoky quartz (Qtz I). This is represented by fault-fill and extensional quartz veins according to the criteria of Robert and Poulsen (2001). Where the V1 vein system uses the S_{1-2} and S_0 structures as infiltration channels, they are denominated by V2 veins (Fig. 4). As these silicification fronts could not move beyond the impermeable carbonaceous phyllite barrier, which prevented further fluid infiltration, massive quartz zones (V1 and V2 veins) concentrated in the hinge zones of folds, and locally brecciated rock portions (Martins et al., 2011) were developed along the BIF–carbonaceous phyllite contact, indicating an increase in P_f relatively to P_L (Figs. 4; 11C). The progressive deformation recrystallized the Qtz I of existing veins, forming milky quartz (Qtz II), which can be observed from the early to the advanced stages of recrystallization, represented by the V3 vein system (Figs. 4 and 5B).

9.2. Hydrothermal fluid evolution

The fluid associated with gold mineralization in the Cabeça de Pedra orebody has a composition in the $H_2O-CO_2-NaCl \pm CH_4$ aqueous–carbonic system. The salinity is low to moderate, averaging ~9 eq. wt.% NaCl for V2 and V3, and ~2 eq. wt.% NaCl for the V1 vein systems, respectively (Fig. 8A, B). The volume percentage of the volatile phase in all FIs is about 10 to 15%, indicating that the fluid was homogeneous with no evidence of boiling (Roedder, 1984).

The diagram T_{dec} vs salinity (Fig. 8A) shows that in V1 and V2 vein systems the salinity varies in the same temperature range. The data are grouped in two families, with variations of 0 to 4 eq. wt.% NaCl for V1, and from 7 to 13 eq. wt.% NaCl for V2. For the case of the V3 vein system (Fig. 8B, C), data are grouped with an average salinity of 9 eq. wt.% NaCl. The range of salinity for all three V1, V2 and V3 indicates an increase in salinity as recrystallization of quartz advances. Recrystallization took place during the D_1-D_2 progressive deformation (Lobato et al., 2013; Martins et al., 2011), which may have caused grain boundaries migration, while the quartz crystal structure accommodated the crystalline dislocations (Urai et al., 1986). This process may be observed at different recrystallization stages, starting with fine polygonal crystals in an incipient stage (Fig. 5B), being formed along the edges of smoky quartz crystals, to a more advanced stage during which veins of milky quartz are developed (Figs. 4 and 5B).

The color of the smoky quartz is due mainly to the large amount of FIs, most of which contain very fine particles of carbonaceous matter, particularly present in type IA FIs, indicated by the Raman spectra (Fig. 6H). The change in color (smoky quartz to milky quartz), takes place once quartz is recrystallized, and results from the migration of carbonaceous matter to the edges of the crystals (Schmatz and Urai, 2011). The water loss in FI during recrystallization (Drury and Urai, 1990; Schmatz and Urai, 2011), resulting from aqueous FIs accumulating along crystal edges (type III, Fig. 6A and E), may have caused the salinity increase in FIs trapped in recrystallized quartz (Qtz II) leading to higher salinity values observed in V3 veins (Fig. 8B). This also may have been the case for relatively higher salinity values in V2 veins (similar to V3; Fig. 8A), possibly due to the partial recrystallization of Qtz I (Fig. 5B).

Taking into account the vein classification and their FI studies, the fluid evolution for the Cabeça de Pedra orebody of the Lamego deposit is interpreted in two stages, characterizing a fluid that is interpreted to have a metamorphic origin:

- Stage 1 Aqueous–carbonic fluid of low salinity (average 2 eq. wt.% NaCl) with a decrepitation temperature in the range of 200 to >300 °C, represented by type IA FIs trapped in smoky quartz (Qtz I in V1 veins; see the dispersion data in Fig. 8A, D);
- Stage 2 Carbonic–aqueous fluid, with moderate salinity (average 9 eq. wt.% NaCl) with the same range of decrepitation temperature, represented by type IB FIs trapped in recrystallized, milky quartz (Qtz II in V2 and V3 veins; Fig. 8B, D).

An intermediate state between stages 1 and 2 may be observed in Fig. 8C represented by type II FIs, where both low and moderate salinity values are related to the same vein system. The content of CH_4 in all vein systems shows the same dispersion data (Fig. 8D, E, F); CH_4 is represented by T_{mCO_2} , where temperatures less than –56.6 °C indicate a major of CH_4 content in the volatile phase (Van Den Kerkhof, 1990). This suggests that the proportions of the volatile phase components in the fluid have not changed with recrystallization. The same situation applies for density of CO_2 in all veins (Fig. 8E).

Fig. 8F shows different fluid density values for each vein system, which can be explained by the increase of salinity with the advance of recrystallization. The lowest density values represent veins characterized by low salinity (V1 veins; Fig. 8D).

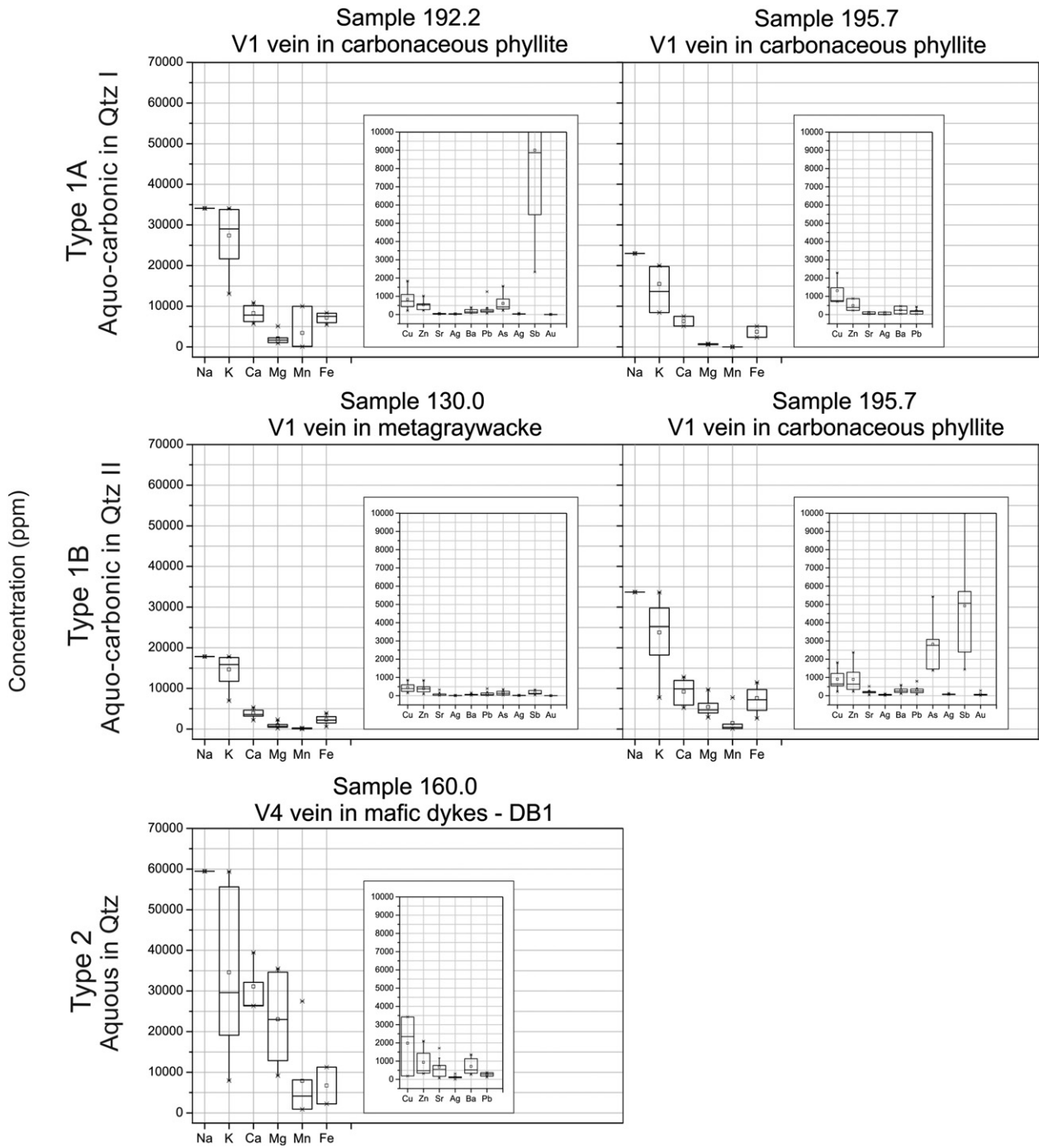


Fig. 10. Diagrams showing metal concentrations obtained from LA-ICP-MS microanalyses of fluid inclusion assemblages and individual fluid inclusions at the Carvoaria Velha gold deposit (Ribeiro et al., 2015), Córrego do Sítio lineament. These results are meant to be compared with data obtained for the Cabeça de Pedra orebody, Lamego deposit.

Considering that the microthermometric data are not accurate to estimate the minimum trapping temperature, since the majority of FIs decrepitated before homogenizing, the arsenopyrite geothermometer was applied, and temperature values calculated between 300 and 375 °C (Fig. 11B). Based on these temperatures, the minimum pressure was estimated to have been 2.6 to 2.8 kbar for inclusions of low salinity (Fig. 11C).

According to Roedder and Bodnar (1980) and Takenouchi and Kennedy (1965), in the H₂O + CO₂ system, pressure increases as the concentration of electrolytes in the solution is higher and the isochores may have different pressures depending on the NaCl

percentage equivalent in solution (Fig. 11C). The complexities of pressure determinations from inclusions containing both carbon dioxide and water might best be illustrated with isochores of moderate salinity (~9 eq. wt.% NaCl). Therefore, calculated pressure values for moderate salinity inclusions are higher (>3500 bar, see Fig. 11C) than for those with low salinity at geothermometer temperature, and they are not compatible with the metamorphic facies mineralogy at Cabeça de Pedra. However, this also indicates that the hydrothermal fluid was subjected to continuous pressure changes (Sibson et al., 1988) that must have favored silica precipitation with gold.

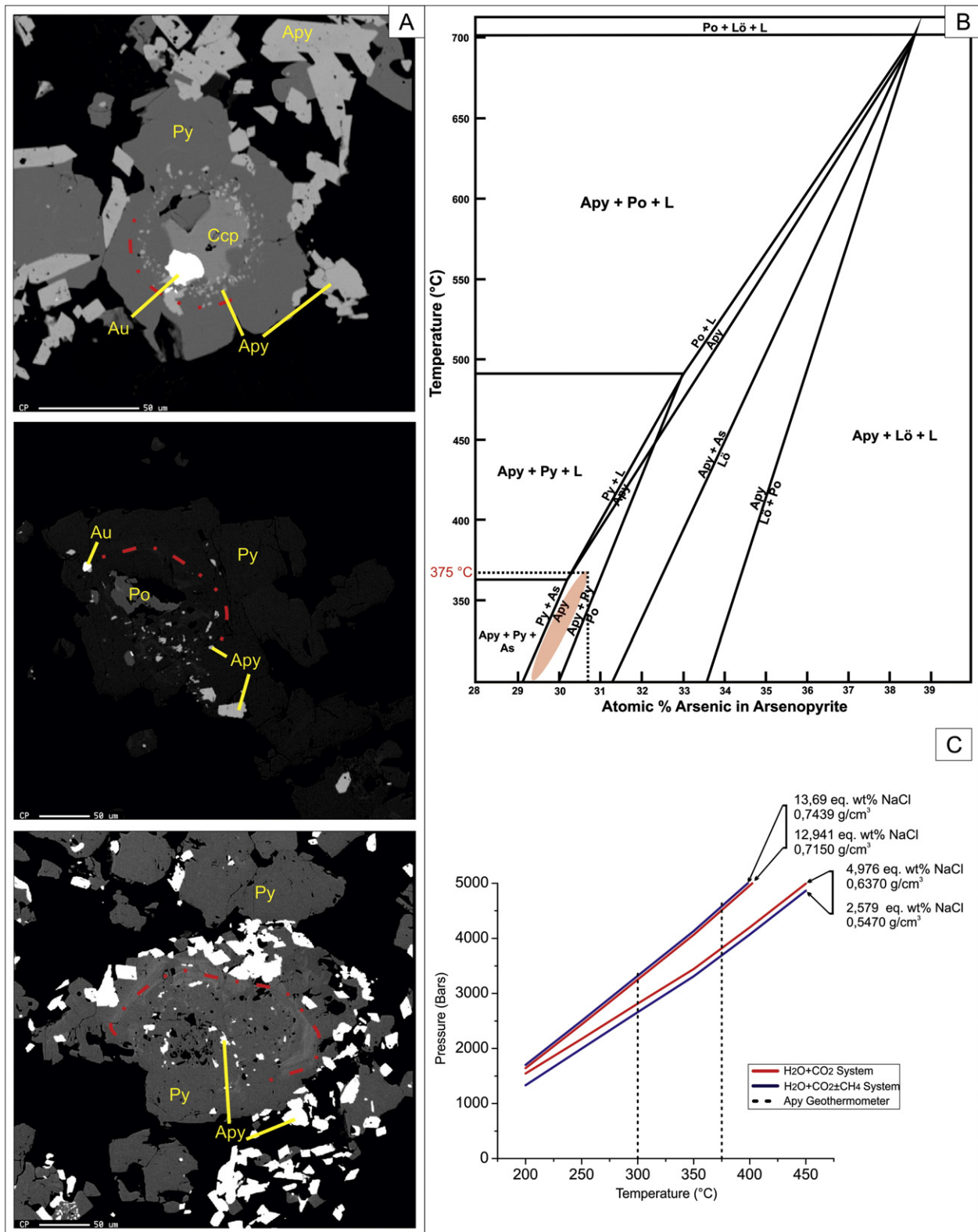


Fig. 11. A) Backscattered scanning image of As-rich pyrite (Py) and arsenopyrite (Apy) crystals showing alteration rims (red lines) with associated gold particles. B) Diagram of Kretschmar and Scott (1976) shows arsenic % atomic concentration vs temperature applied to arsenopyrite geothermometer. Values for this study are represented as a red area. The abbreviations correspond to: Apy – arsenopyrite; Po – pyrrhotite; Py – pyrite and Lö – loellingite. C) Minimum pressure estimates of FI in the H₂O + CO₂ and H₂O + CO₂ ± CH₄ systems, calculated from the intersection of arsenopyrite geothermometer with the isochores. Note the different pressure estimate between the inclusions of low and moderate salinities.

Fluid inclusion studies in different deposits hosted in Archean rocks of the QF region have previously reported high proportions of CH₄ (e.g., Alves, 1995; Godoy, 1994; Lobato et al., 2001b; Ribeiro et al.,

2015; Xavier et al., 2000), due to the hydrolysis reaction of carbonaceous matter ($2C + 2H_2O = CO_2 + CH_4$ or $C + 2H_2 = CH_4 + O_2$) present in the host rocks. In the case of the Cabeça de Pedra orebody, the

Table 7

Composition data of arsenopyrite crystals from mineralized samples of the Cabeça de Pedra orebody, obtained from electron microprobe analysis.

wt.%											Average
As	43.11	42.95	43.25	43.15	43.88	43.35	41.33	42.92	41.72	40.22	42.59
Fe	35.19	35.19	35.04	34.72	35.59	35.49	35.81	35.37	35.71	35.34	35.34
S	22.42	22.53	22.33	21.95	22.10	22.42	22.91	22.11	23.04	23.55	22.54
Total	100.72	100.67	100.62	99.82	101.57	101.26	100.05	100.40	100.46	99.11	100.47
at%											
As	30.20	30.05	30.34	30.58	30.61	30.22	28.90	30.20	29.07	28.17	29.83
Fe	33.06	33.05	33.00	33.02	33.32	33.21	33.61	33.40	33.38	33.22	33.23
S	36.74	36.90	36.67	36.40	36.07	36.58	37.49	36.41	37.55	38.60	36.94
Total	100.00	100.00	100.00	100.00	100.00	100.00	100.00	100.00	100.00	100.00	100.00

maximum CO₂:CH₄ ratio is 4:1 (Table 3), with a maximum CH₄ concentration of 22.6 mol% in the carbonic phase.

9.3. Gold precipitation mechanisms

The processes for gold precipitation in the Cabeça de Pedra orebody must have been:

1. Hydrolysis of carbonaceous matter of both phyllite and BIF, incorporating CH₄ to the fluid and decreasing *f*O₂, causing destabilization of the gold–sulfur complexes;
2. The decrease of the total sulfur concentration in solution and reduced sulfur in the fluid during BIF sulfidation, possibly following reactions: i) FeCO₃siderite + 2H₂S + 1/2O₂ = FeS₂pyrite + CO₂ + 2H₂O (Phillips, 1986); ii) Fe₃O₄magnetite + 6H₂S = 3FeS₂pyrite + 4H₂O + 2H₂ (Phillips and Powell, 2010). Gold precipitates in pyrite, associated with the overgrowth of arsenopyrite, where arsenic precipitation is strongly favored by fluid reduction (Heinrich and Eadington, 1986), and hence As has an association with gold and carbonaceous shales (Phillips and Powell, 2010);
3. The continuous variations in pressure, associated with the formation of faulting and folding, allowed the infiltration of large amounts of fluids, mainly in the hinge zones of BIF (V1 vein system), evolving to breccia-textured massive quartz with free gold. This is particularly well observed along the contact between carbonaceous phyllite and BIF (V2 vein system).

9.4. LA-ICP-MS in fluid inclusions of the Cabeça de Pedra orebody and the Carvoaria Velha deposit, Córrego do Sítio lineament – a comparison

In the Cabeça de Pedra orebody, the high concentration of major elements, such as Na, K, Ca and Mg, in FIs hosted in carbonaceous phyllites and BIF, is similar to that of metamorphic fluids in orogenic gold systems (Ridley and Diamond, 2000). This is a consequence of the salinity increase in FIs in all types of analyzed veins with the order of abundance Na > K > Ca > Mg. The cations K, Ca and Mg are responsible for the lower eutectic temperature (–35 °C) when compared to fluids containing only Na (Borisenco, 1977). Particularly, the enrichment in K and Mg in the fluid reflects the formation of hydrothermal alteration minerals, such as sericite and chlorite, which are typical of proximal alteration zones of metamorphic rocks (Ridley and Diamond, 2000), as described by Martins et al. (2011).

As shown in Table 4 and Fig. 9, Zn has the highest concentration in veins hosted in carbonaceous phyllites, V2 vein (sample 11-7), and V3 veins (up to 3783 ppm) when compared to veins hosted in BIF (up to 612 ppm). Yamaguchi (2002) reports values between 100 and 200 ppm of Zn in black shales from different Archean cratons world while, and suggests hydrothermal activity for these concentrations. Coveney (2003) suggests that the source for Zn enrichment, together with other metals (Ni, Mo, As, Pt, Pd and Au), in Cambrian black shales of south China is hydrothermal fumaroles. On the other hand, Lehmann et al. (2003) interpret that the same black shales are not associated with

volcanic activity, and the authors postulate that metals enrichment is due to direct precipitation from sea water via reduction of the black shales. This may indicate that during hydrothermal fluid interaction to form the Cabeça de Pedra orebody at Lamego, Zn was leached from the carbonaceous phyllite and concentrated in the fluid (Fig. 12B). Copper is more concentrated in veins hosted in carbonaceous phyllite (up to 1293 ppm; Table 4), than in those in BIF (up to 201 ppm; Table 4 and Figs. 9 and 11A). This indicates that as well as Zn, the carbonaceous phyllite was the source of Cu (Large et al., 2011).

The content of As (Table 4) in veins hosted in carbonaceous phyllite (229–975 ppm) is higher than in veins hosted in BIF (37–183 ppm). According to Large et al. (2011), black shales have the capacity of adsorbing As and Au cations in both organic matter particles and diagenetic pyrite, suggesting carbonaceous phyllite as a possible source for these metals in Lamego. Concentration of Au (up to 41 ppm) and Ag (up to 50 ppm) is below the detection limit (Table 4) in the majority of the analyzed veins, indicating that these metals were precipitated and the fluid was metal depleted. Rauchenstein-Martinek et al. (2014) also found extremely low Au (max 0.33 ppm) and Ag (max 2 ppm) results; the authors concluded that metamorphic fluids are commonly unsaturated in gold. A pre-enrichment of gold in the fluid source is essential to generate orogenic deposits, and carbonaceous phyllite and mafic rocks are the most favorable rock types for this process (Large et al., 2011). In the case of the Cabeça de Pedra orebody, gold must have been therefore incorporated in solution during metamorphic devolatilization (Phillips and Powell, 2010; Pitcairn et al., 2006, 2014) of carbonaceous phyllites (Fig. 12A) similarly to what is suggested by Tomkins (2010, 2013a,b) and Large et al. (2011). However, the metabasalt at Lamego may also have been a source of gold, but possibly not for As and certainly not for Sb (Pitcairn et al., 2015).

Fluid inclusions in quartz veins of the Carvoaria Velha deposit, Córrego do Sítio lineament (Ribeiro et al., 2015), show a similar concentration of the elements Na, K, Ca and Mg (Fig. 10) typical of metamorphic fluids (Ridley and Diamond, 2000). The Cu and Sr contents are noticeably higher in veins hosted in mafic dikes (Table 6), with Cu values up to 3420 ppm and Sr up to 545 ppm, when compared to a maximum of 1300 ppm Cu, and 180 ppm Sr in veins hosted in carbonaceous phyllite. These values indicate an important mafic contribution for these metals, but do not exclude carbonaceous phyllite as a possible source (Fig. 13).

Antimony-rich (variation from 5000 to 9000 ppm) inclusions of veins hosted in carbonaceous phyllite at Carvoaria Velha (Table 6 and Fig. 10) suggest leaching of Sb from carbonaceous-dominated host rocks (Fig. 13). However, this contrasts with the abundant prevalence of berthierite (FeSb₂S₄) therein. The presence of both Sb phases, berthierite and stibnite (Ribeiro et al., 2015), and Sb in the fluid must result from the pronounced availability of this metal in the whole rock package at the Córrego do Sítio lineament, which is characterized only by the presence of clastic metasedimentary rocks (Roncato et al., 2015). One must also take into account the high efficiency of Sb solubility in fluids interacting with carbonaceous phyllites (Obolensky et al., 2007). Fan et al. (2004) report an enrichment in Sb (50 to 90 ppm) in

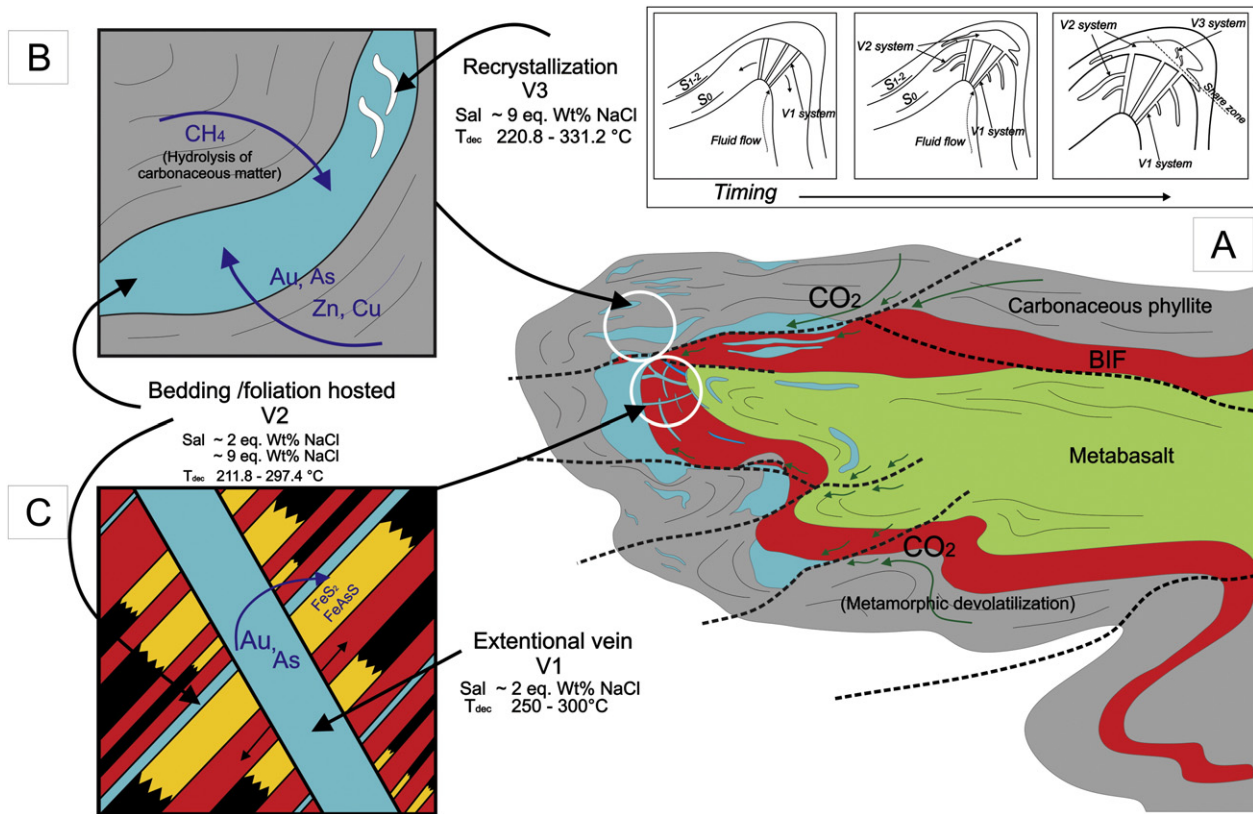


Fig. 12. Schematic hydrothermal fluid model for the gold mineralization at the Cabeça de Pedra orebody, Lamego deposit. At the top-right corner, the sequence of formation of all vein systems and their relationship with the structures is indicated. A) The formation of veins is controlled by folding. Hydrothermal fluid (green arrows) carries cations during metamorphic devolatilization of carbonaceous phyllites (metal source). B) The fluid–rock interaction leaches the metals (Au, Zn, As, Cu) present in the carbonaceous phyllite, incorporating them into the fluid. During the hydrothermal alteration, CH_4 is incorporated into the fluid as a product of the hydrolysis of carbonaceous matter. This process decreases $f\text{O}_2$ and causes destabilization of the gold–sulfur complexes. C) The decrease of sulfur concentration in solution during BIF sulfidation generates the replacement-style of gold precipitation associated with Apy and Py crystals.

black shales from the antimony Xikuangshan deposit, China, suggesting these rocks as the source of metals. Comparing the Xikuangshan concentrations with those obtained in veins from the Carvoaria Velha

deposit, there is a clear increase of 100 to 200 times in the Sb concentration, assuming that the original carbonaceous shale was Sb rich (Fig. 13).

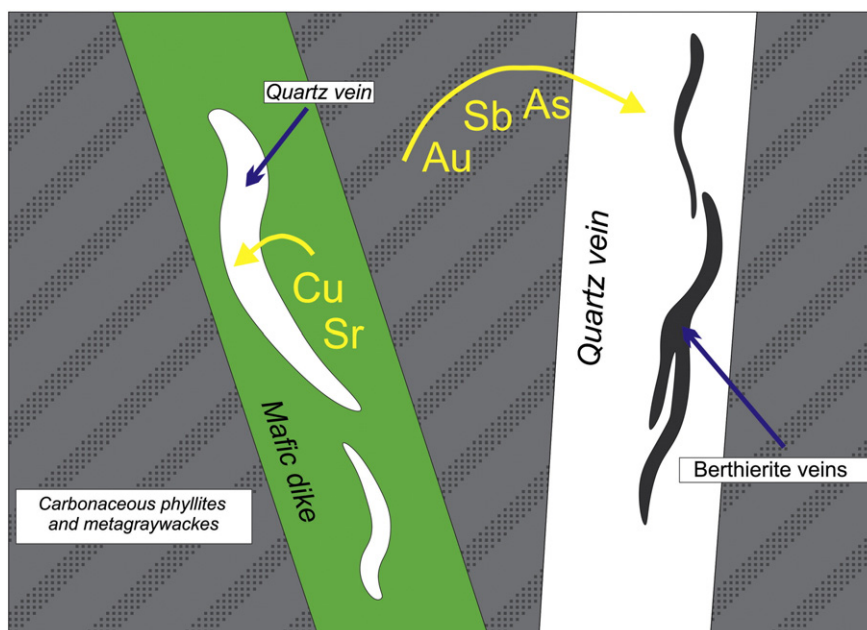


Fig. 13. Schematic model of metal sources at the Carvoaria Velha deposit, Córrego do Sítio lineament. The carbonaceous phyllites and metagraywackes are the source of metals and these are leached during the metamorphic devolatilization process. High concentrations of Sb, As and Au are incorporated into the fluid. Mafic dikes contributed with Cu and Zn.

In relation to As, its behavior is similar to Sb, since it is also in solution (up to 2500 ppm; Table 6), with arsenopyrite being by far the predominant sulfide at Carvoaria Velha (Ribeiro et al., 2015). Fluid As–S–Fe buffering via arsenopyrite + pyrite development Heinrich and Eadington (1986), in a similar temperature range as that of Carvoaria Velha (300 to 375 °C, Ribeiro et al., 2015), was such that both As and Fe (Fig. 11A) were still retained in the fluid phase (Table 6). Gold and silver are depleted in all vein types (Table 6) suggesting that these were precipitated, similar to veins associated with the Cabeça de Pedra orebody, Lamego deposit.

10. Conclusions

Fluid inclusion microthermometric studies combined with LA-ICP-MS in FIs and arsenopyrite geothermometer of different vein systems of the Cabeça de Pedra orebody, at the Lamego orogenic gold deposit, Quadrilátero Ferrífero, allow the following conclusions:

1. Three vein systems are identified, V1, V2 and V3, where the early-stage smoky quartz is referred to as Qtz I, and its recrystallized product Qtz II. The latter constitutes milky, granoblastic crystals.
2. The Cabeça de Pedra orebody was formed from the interaction of low salinity (~2 eq. wt.% NaCl), aqueous–carbonic metamorphic fluids, at temperatures between 200 and 370 °C, and a variable minimum pressure of 2.6 kbar, obtained in Qtz I smoky quartz. The FIs of recrystallized, milky quartz (Qtz II) contain moderate salinities of ~9 eq. wt.% NaCl (Fig. 12A, B). This salinity increase is interpreted as a result of water loss in the FIs during quartz recrystallization Qtz I to Qtz II, when aqueous FIs accumulate along the crystal edges.
3. According to the characteristics of the fluid, T and P conditions (Fig. 11C), and mineralization styles, it is concluded that the orebody was formed in similar conditions described for orogenic gold deposits elsewhere (Groves et al., 1998; Hagemann and Cassidy, 2000), and resembles the proposed models for other gold deposits hosted in Archean rocks of the QF (Lobato et al., 2001b).
4. Fluid infiltration in host rocks must have taken place in several stages, which were closely linked to the formation of the Lamego fold (Fig. 12). Competent rocks, such as BIF, fractured parallel to the axis near the hinge zone, allowing fluid to flow via faults and shear zones (Martins et al., 2011) that acted as channels and created the V1 vein system (Fig. 4). As V1 veins evolved and penetrated along the S_{1-2} foliation and S_0 bedding planes, the V2 veins developed. Silicification was constrained to the BIF–carbonaceous phyllite contacts, since it could not move beyond the impermeable carbonaceous phyllite barrier. Further fluid infiltration was prevented and massive quartz zones were concentrated in the hinge zones of folds, locally forming brecciated portions (Martins et al., 2011) along the BIF–phyllite contact, indicating an increase in P_f relatively to P_L (Fig. 12A). Pressure played a very important role in mineralization, since the large silicification zones that contain the highest gold grades must have been produced due to fluctuations in fluid pressure during infiltration (e.g., Sibson et al., 1988).
5. Gold precipitation was related predominantly to the (i) sulfidation of BIF (Fig. 12C), generating mainly pyrite in association with gold, especially during As enrichment; and (ii) hydrolysis of carbonaceous matter in phyllite, which affected fO_2 , destabilized the sulfur complexes, and resulted in free gold particles (Fig. 12B).
6. The interaction of the hydrothermal fluid with the host rocks has determined the incorporation and depletion of certain elements in the remaining fluid, detected by the LA-ICP-MS technique in FIs. The compositional fluid differences of the Cabeça de Pedra orebody (Lamego) and the Carvoaria Velha deposit (Córrego do Sítio lineament) are closely related to compositional variations of the host metasedimentary units. Carbonaceous phyllites from Lamego provided base metals (i.e., Zn) to the hydrothermal fluid (Fig. 12B), whereas quartz veins associated with the same rock type at the

Carvoaria Velha have significant Sb (Fig. 13). Not only were the original black shales enriched in both Zn and Sb, but they seem to have been sourced differently.

7. For both the Cabeça de Pedra and Carvoaria Velha deposits, the source of Au and As was possibly the pre-enriched carbonaceous phyllite. These elements were probably leached during the metamorphic devolatilization (Large et al., 2011), indicating a local metal and fluid source during gold mineralization (Figs. 12A and 13).
8. The role of carbonaceous phyllites for fluid entrapment and gold concentration has been indicated in the case of some Rio das Velhas greenstone-belt-hosted deposits (e.g., Lobato et al., 2001b; Xavier et al., 2000). They also pointed out the importance of the hydrolysis of carbonaceous matter affecting fO_2 , destabilizing sulfur complexes and enhancing gold precipitation. The present contribution highlights, for the first time in the Rio das Velhas greenstone belt gold deposits, that carbonaceous phyllites also acted as the source of metals, most importantly gold, similarly to what is postulated for example by Gaboury (2013), Large et al. (2011), and Tomkins (2013b), supplied by the black shales of the original Archean stratigraphy. This has enormous exploration implication in this vast region, where chemical and clastic sedimentary rocks dominate the greenstone belt sequence (Baltazar and Zucchetti, 2007).

Acknowledgments

This paper contains results of the M. Sc. dissertation of the first author at the Universidade Federal de Minas Gerais–UFMG, Brazil, who received a scholarship from Coordenação de Aperfeiçoamento de Pessoal de Nível Superior – CAPES. The authors wish to acknowledge AngloGold Ashanti Córrego do Sítio Mineração S/A for their technical, logistic and financial support during our research. Special thanks to all technicians, helpers and geologists in the Lamego mine, especially geologist Fernando Villanova. The main research funds were provided by a project with joint resources from the Brazil's National Council of Technological and Scientific Development – CNPq and Vale. We are also thankful to the School of Earth and Environment, University of Leeds, England; Centro de Pesquisas Prof. Manoel Teixeira da Costa – CPMTc–UFMG; Luis Garcia of the Microanalyses Laboratory of UFMG and Maria Sylvania Dantas for the technical collaboration in the Raman Spectroscopy Lab – Department of Metallurgy and Materials Engineering (UFMG). Finally, we would like to express our appreciation to the reviewers and the editorial staff. LML acknowledges a research grant from the CNPq.

References

- Almeida, F.F.M., 1967. *Origem e evolução da plataforma brasileira*. vol. 241. Departamento Nacional da Produção Mineral. Divisão Geologia Mineral– DNPM, Boletim, Rio de Janeiro, Brasil, p. 36.
- Almeida, F.F.M., Hasui, Y., 1984. *O Pré-Cambriano do Brasil*. Edgar Blücher, São Paulo (378 pp.).
- Alves, J.V., 1995. *Estudo das inclusões fluidas em veios de quartzo da mina de ouro de Sao Bento, Santa Bárbara, MG* (MSc Thesis) Universidade Federal de Minas Gerais, Instituto de Geociências, Belo Horizonte, Brazil.
- Baltazar, O.F., Pedreira, A.J., 1996. Associações de litofácies. In: CPRM–Companhia de Pesquisa de Recursos Minerais. Projeto Rio das Velhas–Texto Explicativo do Mapa Geológico Integrado, escala 1:100.000. Departamento Nacional de Produção Mineral/CPRM–Serviço Geológico do Brasil, Belo Horizonte, p. 43–48.
- Baltazar, O.F., Pedreira, A.J., 1998. Associações litofaciológicas. In: M. Zucchetti and O.F. Baltazar (Eds.), Projeto Rio das Velhas–Texto Explicativo do Mapa Geológico Integrado, escala 1:100.000. 2nd edition, Departamento Nacional de Produção Mineral/CPRM–Serviço Geológico do Brasil, Belo Horizonte, p. 43–47.
- Baltazar, O.F., Zucchetti, M., 2007. Lithofacies associations and structural evolution of the Archean Rio das Velhas greenstone belt, Quadrilátero Ferrífero, Brazil: a review of the regional setting of gold deposits. *Ore Geol. Rev.* 32, 471–499.
- Belo de Oliveira, O.A., Vieira, M.B.H., 1987. Aspectos da deformação dúctil e progressiva no Quadrilátero Ferrífero. 4th. Simpósio de Geologia de Minas Gerais. Sociedade Brasileira de Geologia, Belo Horizonte, Brazil, pp. 237–253.
- Borisenko, A.S., 1977. Study of the salt composition of solutions of gas–liquid inclusions in minerals by the cryometric method. *Geol. Geofiz.* 18 (8), 16–27.
- Bowers, T.S., Helgeson, H.C., 1983. Calculation of the thermodynamic and geochemical consequences of nonideal mixing in the system H_2O – CO_2 –NaCl on phase relations

- in geological systems: equation of state for H_2O-CO_2-NaCl fluids at high pressures and temperatures. *Geochim. Cosmochim. Acta* 47, 1247–1275.
- Brito Neves, B.B., 2011. The Paleoproterozoic in the South-American continent: diversity in the geologic time. *J. S. Am. Earth Sci.* 32, 270–286.
- Brown, P.E., Hagemann, S.G., 1995. MacFlinCor and its application to fluids in Archean lode-gold deposits. *Geochim. Cosmochim. Acta* 59, 3943–3952.
- Burke, E.A.J., 2001. Raman microspectrometry of fluid inclusions. *Lithos* 55, 139–158.
- Carneiro, M.A., 1994. Geocronologia e Geoquímica do Complexo Bonfim. Unpublished Ph.D. thesis, Universidade de São Paulo, 350 pp.
- Coveney, R.M., 2003. Re-Os dating of polymetallic Ni–Mo–PGE–Au mineralization in Lower Cambrian black shales of South China and its geological significance – a discussion. *Econ. Geol.* 98, 661–662.
- Dorr II, J.V., 1969. Physiographic, stratigraphic and structural development of the Quadrilátero Ferrífero, Minas Gerais, Brazil. United States Geological Survey Professional Paper 614-A (110 pp.).
- Dorr II, J.V., Gair, J.E., Pomeroy, J.B., Rynearson, G.A., 1957. Revisão da estratigrafia pré-cambriana do Quadrilátero Ferrífero, Brasil. Departamento Nacional da Produção Mineral, Divisão de Fomento da Produção Mineral, Avulso vol. 81 (31 pp.).
- Drury, M.R., Urai, J.L., 1990. Deformation-related recrystallization processes. *Tectonophysics* 172, 235–253.
- Fan, D., Zhang, T., Ye, J., 2004. The Xikuangshan Sb deposit hosted by the Upper Devonian black shale series, Hunan, China. *Ore Geol. Rev.* 24, 121–133.
- Frezzotti, M.L., Tecce, F., Casagli, A., 2012. Raman spectroscopy for fluid inclusion analysis. *J. Geochim. Explor.* 112, 1–20.
- Gaboury, D., 2013. Does gold in orogenic deposits come from pyrite in deeply buried carbon-rich sediments?: Insight from volatiles in fluid inclusions. *Geology* 41, 1207–1210.
- Gair, J.E., 1962. Geology and ore deposit of the Nova Lima and Rio Acima quadrangles, Minas Gerais, Brazil. United States Geological Survey Professional Paper 341-A (67 pp.).
- Godoy, M.L.S., 1994. Evolução tectono-metamórfica da mineralização aurífera de Raposos (MG) (MSc Thesis) Universidade Estadual Paulista, Instituto Geociências Ciências Exatas, Rio Claro, Brazil.
- Goldfarb, R.J., Groves, D.I., Gardoll, S., 2001. Orogenic gold and geologic time: a global synthesis. *Ore Geol. Rev.* 18, 1–75.
- Goldfarb, R.J., Baker, T., Dube, B., Groves, D.I., Hart, C.J.R., Gosselin, P., 2005. Distribution, character, and genesis of gold deposits in metamorphic terranes. In: Hedenquist, J.W., Thompson, J.F.H., Goldfarb, R.J., Richards, J.P. (Eds.), *Economic Geology. 100th Anniversary Volume 1905–2005*. Society of Economic Geologists, Littleton, Colorado, pp. 407–p. 450.
- Goldstein, R.H., Reynolds, T.J., 1994. Systematics of fluid inclusions in diagenetic minerals. *SEPM Short Course 31*. The Mineralogical Association of Canada, Tulsa (199 pp.).
- Gross, G.A., 1980. A classification of iron formations based on depositional environments. *Can. Mineral.* 18, 215–222.
- Groves, D.I., Goldfarb, R.J., Gebre-Mariam, M., Hagemann, S.G., Robert, F., 1998. Orogenic gold deposits: a proposed classification in the context of their crustal distribution and relationship to other gold deposit types. *Ore Geol. Rev.* 13, 7–27.
- Guillong, M., Meier, D.L., Allan, M.M., Heinrich, C.A., Yardley, B.W.D., 2008. Appendix 6: silts: a Matlab-based program for the reduction of laser ablation ICM-MS data of homogeneous materials and inclusions: Vancouver, B.C. Mineralogical Association of Canada Short Course 40.
- Guimarães, D., 1931. Contribuição à geologia do Estado de Minas Gerais. *Boletim vol. 55*. Departamento Nacional da Produção Mineral, Rio de Janeiro, Brazil, pp. 1–36.
- Hagemann, S.G., 1993. The Wiluna Lode-gold Deposits, Western Australia: A Case Study of a High Level Archean Lode-gold System (Ph.D. thesis) Univ. Western Australia.
- Hagemann, S.G., Cassidy, K.F., 2000. Archean orogenic lode gold deposits. In: Hagemann, S.G., Brown, P.E. (Eds.), *Gold in 2000 Reviews in Economic Geology 13*. Society of Economic Geologists, pp. 9–68.
- Heinrich, C., Eadington, P.J., 1986. Thermodynamic predictions of the hydrothermal chemistry of arsenic, and their significance for the paragenetic sequence of some cassiterite–arsenopyrite–base metal sulphide deposits. *Econ. Geol.* 81, 511–529.
- Herz, N., 1970. Gneissic and igneous rocks of the Quadrilátero Ferrífero, Minas Gerais, Brazil. United States Geological Survey Professional Paper 641-B (58 pp.).
- Herz, N., 1978. Metamorphic rocks of the Quadrilátero Ferrífero, Minas Gerais, Brazil. United States Geological Survey Professional Paper 641-C (81 pp.).
- Jacobs, G.K., Kerrick, D.M., 1981. Methane: an equation of state with application to the ternary system $H_2O-CO_2-CH_4$. *Geochim. Cosmochim. Acta* 45, 607–614.
- Junqueira, P.A., Lobato, L.M., Ladeira, E.A., Simões, E.J.M., 2007. Structural control and hydrothermal alteration at the BIF-hosted Raposos lode-gold deposit, Quadrilátero Ferrífero, Brazil. *Ore Geol. Rev.* 32, 629–650.
- Klein, C., Ladeira, E.A., 2000. Petrology and geochemistry of some proterozoic banded iron-formations of the Quadrilátero Ferrífero, Minas Gerais, Brazil. *Econ. Geol.* 95, 405–428.
- Kretschmar, U., Scott, S.D., 1976. Phase relations involving arsenopyrite in the system Fe–As–S and their application. *Can. Mineral.* 14, 364–386.
- Ladeira, E.A., Viveiros, J.M.F., 1984. Hipótese sobre a estruturação do Quadrilátero Ferrífero com base nos dados disponíveis. *Sociedade Brasileira Geologia, Núcleo de Minas Gerais, Boletim vol. 4* (24 pp.).
- Large, R.R., Bull, S.W., Maslennikov, V.V.A., 2011. Carbonaceous sedimentary source-rock model for Carlin-type and orogenic gold deposits. *Econ. Geol.* 106, 331–358.
- Lehmann, B., Mao, J., Shengrong, L., Zhang, G., Zeng, M., 2003. Re-Os dating of polymetallic Ni–Mo–PGE–Au mineralization in Lower Cambrian black shales of South China and its geological significance – a reply. *Econ. Geol.* 98, 663–665.
- Lima, L.C., 2012. Depósito lode Au–As–Sb Laranjeiras, em metatúrbidos do Grupo Nova Lima, Quadrilátero Ferrífero, Minas Gerais (M.Sc. thesis), Instituto Geociências, Universidade Federal de Minas Gerais, Belo Horizonte, Brasil (306 pp.).
- Lobato, L.M., Vieira, F.W., 1998. Styles of hydrothermal alteration and gold mineralization associated with Nova Lima Group of the Quadrilátero Ferrífero: part II, the Archean mesothermal gold-bearing system. *Rev. Bras. Geosci.* 28, 355–366.
- Lobato, L.M., Vieira, F.W.R., Ribeiro-Rodrigues, L.C., Pereira, L.M.M., Menezes, M.G., Junqueira, P.A., Pereira, S.L.M., 1998. Styles of hydrothermal alteration and gold mineralization associated with Nova Lima Group of the Quadrilátero Ferrífero: part I, description of selected gold deposits. *Rev. Bras. Geosci.* 28, 339–354.
- Lobato, L.M., Ribeiro-Rodrigues, L.C., Zucchetti, M., Noce, C.M., Baltazar, O.F., Silva, L.C., Pinto, C.P., 2001a. Brazil's premier gold province. Part I: the tectonic, magmatic and structural setting of the Archean Rio das Velhas greenstone belt, Quadrilátero Ferrífero. *Mineral. Deposita* 36, 228–248.
- Lobato, L.M., Ribeiro-Rodrigues, L.C., Vieira, F.W.R., 2001b. Brazil's premier gold province. Part II: geology and genesis of gold deposits in the Archean Rio das Velhas greenstone belt, Quadrilátero Ferrífero. *Mineral. Deposita* 36, 249–277.
- Lobato, L.M., Martins, B.S., Rosière, C.A., Figueiredo e Silva, R.C., Lemos, L.H.A., Villanova, F.L.S.P., Amaral, L.F.S., 2013. Depth variation characteristics at the Carruagem orebody, Archean BIF-hosted Lamego gold deposit, Quadrilátero Ferrífero, Brazil. Paper Presented at the 12th SGA Biennial Meeting – Mineral Deposit Research for a High-tech World, Uppsala, Sweden, 12–15 August.
- Loczy, L., Ladeira, E.A., 1976. *Geologia Estrutural e Introdução à Geotectônica*. Edgar Blücher, São Paulo (528 pp.).
- Machado, N., Carneiro, M.A., 1992. U–Pb evidence of late Archean tectono-thermal activity in the southern São Francisco shield, Brazil. *Can. J. Earth Sci.* 29, 2341–2346.
- Machado, N., Noce, C.M., De Oliveira, O.A.B., Ladeira, E.A., 1989a. Evolução Geológica do Quadrilátero Arqueano e Proterozóico Inferior com base em geocronologia U/Pb. 5. Simpósio de Geologia de Minas Gerais, Belo Horizonte, 1989. Sociedade Brasileira de Geologia, núcleo Minas Gerais, Extended Abstract Volume, pp. 1–5.
- Machado, N., Schrank, A., Abreu, F.R., Knauer, L.G., Almeida-Abreu, P.A., 1989b. Resultados preliminares da geocronologia U–Pb na Serra do Espinhaço Meridional. 15th Simpósio de Geologia de Minas Gerais. Sociedade Brasileira de Geologia, Belo Horizonte, pp. 171–174.
- Marshak, S., Alkmim, F.F., 1989. Proterozoic contraction/extension tectonics of the southern São Francisco region, Minas Gerais, Brazil. *Tectonics* 8, 171–174.
- Martins, B.S., 2011. Controle da mineralização aurífera de Lamego, Sabará, Quadrilátero Ferrífero (MG). M.Sc. thesis, Universidade Federal de Minas Gerais, Belo Horizonte, Brazil 250 pp.
- Martins Pereira, S.L., Lobato, L.M., Ferreira, J.E., Jardim, E.C., 2007. Nature and origin of the BIF-hosted São Bento gold deposit, Quadrilátero Ferrífero, Brazil, with special emphasis on structural controls. *Ore Geol. Rev.* 32, 571–595.
- Martins, B.S., Rosière, C.A., Lobato, L.M., Figueiredo e Silva, R.C., Baars, F.J., Tschiedel, M.W., Oliveira, H., Penha, U.C., 2011. Mineralization control of the Lamego Gold Deposit, Sabará, Quadrilátero Ferrífero, Minas Gerais, Brazil. Society for Geology Applied to Mineral Deposits (SGA) Biennial Meeting, 11th, Proceedings, Antofagasta, Chile.
- Morey, A.A., Tomkins, A.G., Bierlein, F.P., Weinberg, R.F., Davidson, G., 2008. Bimodal distribution of gold in pyrite and arsenopyrite: examples from the Archean Boorara and Bardoc shear systems, Yilgarn Craton, Western Australia. *Econ. Geol.* 103, 599–614.
- Noce, C.M., 1995. Geocronologia dos eventos magmáticos, sedimentares e metamórficos na região do Quadrilátero Ferrífero, Minas Gerais. Unpublished Ph.D. thesis, Universidade de São Paulo, Brazil, 128 pp.
- Noce, C.M., Machado, N., Teixeira, W., 1998. U–Pb geochronology of gneisses and granitoids in the Quadrilátero Ferrífero (southern São Francisco craton): age constraints for Archean and Paleoproterozoic magmatism and metamorphism. *Rev. Bras. Geosci.* 28, 95–102.
- Noce, C.M., Dantas, E.L., Lobato, L.M., Zucchetti, M., Baltazar, O.F., 2002. Múltiplos eventos de vulcanismo no greenstone belt Rio das Velhas, Quadrilátero Ferrífero (MG): novos dados U–Pb, implicações geotectônicas e metalogênicas. 41th Congresso Brasileiro de Geologia. Sociedade Brasileira de Geologia, João Pessoa p. 522.
- Noce, C.M., Tassinari, C.G., Lobato, L.M., 2007. Geochronological framework of the Quadrilátero Ferrífero, with emphasis on the age of gold mineralization hosted in Archean greenstone belts. *Ore Geol. Rev.* 32, 500–510.
- Obolensky, A.A., Gushchina, L.V., Borisenko, A.S., Borovikov, A.A., Pavlova, G.G., 2007. Antimony in hydrothermal processes: solubility, conditions of transfer, and metal-bearing capacity of solutions. *Russ. Geol. Geophys.* 48, 992–1001.
- Oliveira, G.A.I., Caiafa, P.L., Vial, D.S., 1983. Excursão à mina de ouro de Morro Velho. *Sociedade Brasileira de Geologia. Núcleo de Minas Gerais Boletim vol. 3* pp. 497–505.
- O'Rourke, J.E., 1957. The stratigraphy of metamorphic rocks of the Rio de Pedras and Gandarela quadrangles, Minas Gerais, Brazil (PhD thesis), University of Wisconsin, Wisconsin (106 pp.).
- Pedreira, A.J., Silva, S.L., 1996. Sistemas deposicionais do greenstone belt Rio das Velhas, Quadrilátero Ferrífero, Minas Gerais. 39th Congresso Brasileiro de Geologia. Sociedade Brasileira de Geologia, Salvador, pp. 138–140.
- Phillips, G.N., 1986. Geology and alteration in the Golden Mile, Kalgoorlie. *Econ. Geol.* 81, 779–808.
- Phillips, G.N., Powell, R., 2010. Formation of gold deposits: a metamorphic developmental model. *J. Metamorph. Geol.* 28, 689–718.
- Pitcairn, I.K., Teagle, D.A.H., Craw, D., Olivo, G.R., Kerrich, R., Brewer, T.S., 2006. Sources of metals and fluids in orogenic gold deposits: insights from the Otago and Alpine Schists, New Zealand. *Econ. Geol.* 101, 1525–1546.
- Pitcairn, I.K., Craw, D., Teagle, D.A.H., 2014. The gold conveyor belt: large-scale gold mobility in an active orogeny. *Ore Geol. Rev.* 62, 129–142.
- Pitcairn, I.K., Craw, D., Teagle, D.A.H., 2015. Metabasalts as sources of metals in orogenic gold deposits. *Mineral. Deposita* 50, 373–390.
- Ramsay, J.G., 1967. *Folding and Fracturing of Rocks*. McGraw-Hill, New York.

- Rauchenstein-Martinek, K., Wagner, T., Wälle, M., Heinrich, C.A., 2014. Gold concentrations in metamorphic fluids: a LA-ICPMS study of fluid inclusions from the Alpine orogenic belt. *Chem. Geol.* 385, 70–83.
- Renger, F.S., Noce, C.M., Romano, A.W., Machado, N., 1994. Evolução sedimentar do Supergrupo Minas: 500 Ma de registro geológico no Quadrilátero Ferrífero, Minas Gerais, Brasil. *Geonomos* 2, 1–11.
- Ribeiro, Y., Figueiredo e Silva, R.C., Lobato, L.M., Lima, L.C., Rios, F.J., Hagemann, S.G., Cliff, J., 2015. Fluid inclusion and sulfur and oxygen isotope studies on quartz–carbonate–sulfide veins of the Carvoaria Velha deposit, Córrego do Sítio gold lineament, Quadrilátero Ferrífero, Minas Gerais, Brazil. *Ore Geol. Rev.* 67, 11–33.
- Ribeiro-Rodrigues, L.C., 1998. Gold in Archaean banded iron formation of the Quadrilátero Ferrífero, Minas Gerais, Brazil – the Cuibá mine (Ph.D. Thesis), Aachener Geowissenschaftliche Beiträge Band 27. Aachen University of Technology. Augustinus Verlag (264 pp.).
- Ribeiro-Rodrigues, L.C., Oliveira, C.G., Friedrich, G., 2007. The Archean BIF-hosted Cuibá Gold deposit, Quadrilátero Ferrífero, Minas Gerais, Brazil. *Ore Geol. Rev.* 32, 543–570.
- Ridley, J.R., Diamond, L.W., 2000. Chapter 4 – fluid chemistry of orogenic lode gold deposits and implications for genetic models. *SEG Rev.* 13, 141–162.
- Robert, F., Poulsen, K.H., 2001. Vein formation and deformation in greenstone gold deposits. In: Richards, J.P., Tosdal, R.M. (Eds.), *Structural Controls on Ore Genesis. Reviews in Economic Geology* 14, pp. 111–156.
- Roedder, E., 1984. Fluid inclusions. *Rev. Mineral.* 12. Mineralogical Society of America, p. 646.
- Roedder, E., Bodnar, R.J., 1980. Geologic pressure determinations from fluid inclusion studies. *Annu. Rev. Earth Planet. Sci.* 8, 263–301.
- Roncato Jr., J.G., Lobato, L.M., Lima, L.C., Porto, C.G., Figueiredo e Silva, R.C., 2015. Metaturbidite-hosted gold deposits, Córrego do Sítio Lineament, Quadrilátero Ferrífero, Brazil. *Braz. J. Geol.* 45, 5–22.
- Russell-Wood, A.J., 1984. Colonial Brazil: the gold cycle, c. 1690–1750. *The Cambridge History of Latin America* vol. II. Cambridge University Press, pp. 547–600.
- Sales, M., 1998. The geological setting of the Lamego iron-formation-hosted gold deposit, Quadrilátero Ferrífero district, Minas Gerais, Brazil. Unpublished M.Sc. Thesis, Queens University, Hamilton, Canada, 182 pp.
- Schmatz, J., Urai, J.L., 2011. The interaction of migrating grain boundaries and fluid inclusions in naturally deformed quartz: a case study of a folded and partly recrystallized quartz vein from the Hunsrück Slate, Germany. *J. Struct. Geol.* 33, 468–480.
- Schrank, A., Machado, N., 1996. Idades U–Pb em monazitas e zircões do distrito aurífero de Caeté, da mina de Cuibá e do depósito de Carrapato–Quadrilátero Ferrífero (MG). 39th Congresso Brasileiro de Geologia. Sociedade Brasileira de Geologia, Salvador, pp. 473–475.
- Schrank, A., Machado, N., Stern, R., 2002. Eventos no Arqueano com base em idades U/Pb–SHRIMP de zircões detriticos em metassedimentos da mina de Morro Velho–Quadrilátero Ferrífero–Minas Gerais. 41th Congresso Brasileiro de Geologia. Sociedade Brasileira de Geologia, João Pessoa, p. 527.
- Shepherd, T.J., Rankin, A.H., Alderton, D.H.M., 1985. *A Practical Guide to Fluid Inclusion Studies*. Blackie and Son, Glasgow (239 pp.).
- Sibson, R.H., Robert, F.K., Poulsen, H., 1988. High-angle reverse faults, fluid–pressure cycling, and mesothermal gold–quartz deposits. *Geology* 16, 551–555.
- Takenouchi, S., Kennedy, G.C., 1965. The solubility of carbon dioxide in NaCl solutions at high temperatures and pressures. *Am. J. Sci.* 263, 445–455.
- Teixeira, W., Carneiro, M.A., Noce, C.M., Machado, N., Sato, K., Taylor, P.N., 1996. Pb, Sr and Nd isotope constraints on the Archean evolution of gneissic–granitoid complexes in the southern São Francisco craton, Brazil. *Precambrian Res.* 78, 151–164.
- Thiéry, R., van der Kerkhof, A.F., Dubessy, F., 1994. vX properties of CH₄–CO₂ and CO₂–N₂ fluid inclusions: modeling for T–318C and P–400 bar. *Eur. J. Mineral.* 6, 753–771.
- Tomkins, A.G., 2010. Windows of metamorphic sulfur liberation in the crust: implications for gold deposit genesis. *Geochim. Cosmochim. Acta* 74, 3246–3259.
- Tomkins, A.G., 2013a. A biogeochemical influence on the secular distribution of orogenic gold. *Econ. Geol.* 108, 193–197.
- Tomkins, A.G., 2013b. On the source of orogenic gold. *Geology* 41, 1255–1256.
- Urai, J.L., Means, W.D., Lister, G.S., 1986. Dynamic recrystallization of minerals. In: Hobbs, B.E., Heard, H.C. (Eds.), *Mineral and Rock Deformation: Laboratory Studies; The Paterson Volume. Geophysical Monograph* vol. 36, pp. 161–199.
- Van Den Kerkhof, A.M., 1990. Isochoric phase diagrams in the systems CO₂–CH₄ and CO₂–N₂: application to fluid inclusions. *Geochim. Cosmochim. Acta* 54, 621–629.
- Vial, D.S., Abreu, G.C., Schubert, G., Ribeiro-Rodrigues, L.C., 2007a. Smaller gold deposits in the Archean Rio das Velhas greenstone belt, Quadrilátero Ferrífero, Brazil. *Ore Geol. Rev.* 32, 651–673.
- Vial, D.S., De Witt, E., Lobato, L.M., Thorman, C.H., 2007b. The geology of the Morro Velho gold deposit in the Archean Rio das Velhas greenstone belt, Quadrilátero Ferrífero, Brazil. *Ore Geol. Rev.* 32, 511–542.
- Vieira, F.W.R., 1991. Textures and processes of hydrothermal alteration and mineralization in the Nova Lima Group, Minas Gerais, Brazil. Paper Presented at the Brazil Gold'91, Belo Horizonte.
- Vieira, F.W.R., Oliveira, G.A.I., 1988. Geologia do distrito aurífero de Nova Lima, Minas Gerais. In: Schobenhau-Filho, C., Coelho, C.E.S. (Eds.), *Metals básicos não ferrosos, ouro e alumínio Principais Depósitos Minerais do Brasil* vol. 3. Departamento Nacional da Produção Mineral/Companhia Vale do Rio Doce, Brasília, Brazil, pp. 377–391.
- Villanova F.L.S.P., 2011. Mapeamento Geológico em escala 1:5.000 da superfície e região circunvizinha da Mina Lamego, Sabará, Minas Gerais. Universidade Federal de Minas Gerais.
- Xavier, R.P., Toledo, C.L.B., Taylor, B.E., Schrank, A., 2000. Fluid evolution and gold deposition at the Cuibá mine, SE Brazil: fluid inclusions and stable isotope geochemistry of carbonates. *Rev. Bras. Geosci.* 30 (2), 337–341.
- Yamaguchi, K., 2002. *Geochemistry of Archean–Paleoproterozoic Black Shales: The Early Evolution of the Atmosphere, Oceans, and Biosphere* (PhD. thesis) The Pennsylvania State University.
- Zucchetti, M., Baltazar, O.F., 1998. Projeto Rio das Velhas–Texto Explicativo do mapa geológico integrado, escala 1:100.000, 2nd ed. Belo Horizonte: Departamento Nacional da Produção Mineral–Companhia de Pesquisa de Recursos Minerais, 121 pp.
- Zucchetti, M., Baltazar, O.F., 2000. Rio das Velhas Greenstone Belt lithofacies associations, Quadrilátero Ferrífero, Minas Gerais, Brazil. 31st International Geological Congress, Rio de Janeiro, Brazil. CD-ROM.